The Astronomical Journal, 138:1171–1191, 2009 October doi:10.1088/0004-6256/138/4/1171

LITHIUM IN THE INTERMEDIATE-AGE OPEN CLUSTER, NGC 3680

Barbara J. Anthony-Twarog[1], Constantine P. Deliyannis[2,3], Bruce A. Twarog[1,3], Kevin V. Croxall[2], and Jeffrey D. Cummings[2]

[1] Department of Physics and Astronomy, University of Kansas, Lawrence, KS 66045-7582, USA; bjat@ku.edu, btwarog@ku.edu
[2] Department of Astronomy, Indiana University, Bloomington, IN 47405-7105, USA; con@astro.indiana.edu, kcroxall@indiana.edu, jdcummi@astro.indiana.edu
Received 2009 March 27; accepted 2009 August 13; published 2009 September 11

ABSTRACT

High-dispersion spectra centered on the Li 6708 Å line have been obtained for 70 potential members of the intermediate-age open cluster NGC 3680, with an emphasis on stars in the turnoff region of the cluster color–magnitude diagram (CMD). A measurable Li abundance has been derived for 53 stars, 39 of which have radial velocities and proper motions consistent with cluster membership. After being transferred to common temperature and abundance scales, previous Li estimates have been combined to generate a sample of 49 members, 40 of which bracket the cluster Li-dip. Spectroscopic elemental analysis of eight giants and five turnoff stars produces [Fe/H] $= -0.17 \pm 0.07$ (sd) and -0.07 ± 0.02 (sd), respectively. We also report measurements of Ca, Si, and Ni which are consistent with scaled-solar ratios within the errors. Adopting [Fe/H] $= -0.08$ (Section 3.6), Y^2 isochrone comparisons lead to an age of 1.75 ± 0.1 Gyr and an apparent modulus of $(m - M) = 10.30 \pm 0.15$ for the cluster, placing the center of the Li-dip at 1.35 ± 0.03 $M_{\odot}$. Among the giants, five of the nine cluster members are now known to have measurable Li with A(Li) near 1.0. A combined sample of dwarfs in the Hyades and Praesepe is used to delineate the Li-dip profile at 0.7 Gyr and [Fe/H] $= +0.15$, establishing its center at 1.42 ± 0.02 $M_{\odot}$ and noting the possible existence of a secondary dip on its red boundary. When evolved to the typical age of the clusters NGC 752 (age = 1.45 Gyr, $(m - M) = 8.4$), IC 4651 (age = 1.5 Gyr, $(m - M) = 10.4$), and NGC 3680, the Hyades/Praesepe Li-dip profile reproduces the observed morphology of the combined Li-dip within the CMDs of the intermediate-age clusters while implying a metallicity dependence for the central mass of the Li-dip given by $M/M_{\odot} = 1.38 \pm 0.04 + 0.4 \pm 0.2$ [Fe/H]. The implications of the similarity of the Li-dichotomy among giants in NGC 752 and IC 4651 and the disagreement with the pattern among NGC 3680 giants are discussed.

Key words: open clusters and associations: individual (NGC 752, NGC 3680, IC 4651, Praesepe, Hyades) – stars: abundances – techniques: spectroscopic

1. INTRODUCTION

Open clusters are studied for a variety of reasons, ranging from their intended use as probes of the structural and chemical evolution of the Galaxy (Friel et al. 2002; Yong et al. 2005; Sestito et al. 2008) to delineation of the finer details of stellar structure and evolution (Meibom et al. 2002; VandenBerg & Stetson 2004). While lithium is an element with clear cosmological origins and ramifications, studies of lithium in open clusters predominantly emphasize its role within stellar evolution, though insights gained from these investigations could have an indirect impact upon our understanding of the cosmological parameters (Sestito & Randich 2005; Korn et al. 2006; Deliyannis 2000). Lithium, boron, and beryllium are relatively fragile nuclei. Attrition of lithium from the presumed initial value of A(Li) = 3.30 implied by meteoritic abundances (Anders & Grevesse 1989) and very young star clusters, is expected in the internal layers of stars or protostars where the temperatures exceed $\sim 2.5 \times 10^6$ K, above which Li burns via proton capture to ^{4}He. Over a star's lifetime, the integrated effect of any structural features that put surface layers in contact with the deeper layers at or above this temperature will be expressed in the depletion of surface Li. The surface Li abundance can also be enhanced if radiative acceleration pushes it into the surface convection zone (SCZ; Richer & Michaud 1993; Deliyannis et al. 2002) or if a deepening convection zone dredges up previously diffused Li (Deliyannis et al. 1990; Sills & Deliyannis 2000).

Standard[4] stellar evolution theory (SSET) predicts the attrition of Li as a function of stellar mass, age, and composition. Low-mass pre-main-sequence models evolving down the Hayashi track develop high enough temperatures at the base of the SCZ so that energetic protons destroy Li there, thereby depleting the surface Li abundance. Lower stellar mass implies a deeper and longer-lived SCZ, which implies more Li depletion; there is little Li depletion for models reaching the zero-age main sequence (ZAMS) as A, F, and G dwarfs, while Li depletion is more severe for K and cooler spectral types (e.g., Pinsonneault 1997). Li depletion ceases as the SCZ recedes toward the surface and its base cools. Independent of the details of the (standard) input physics, SSET *robustly* predicts that no further Li depletion occurs during the MS for AFG dwarfs (e.g., Proffitt & Michaud 1989; Deliyannis et al. 1990; Pinsonneault et al. 1990; Swenson et al. 1994; Chaboyer et al. 1995), whereas KM dwarfs can continue to deplete Li as they evolve beyond the ZAMS. The predicted Li–T_e relation is modified very slightly as models evolve to slightly higher T_e over time. Higher-metallicity models have deeper convection and deplete more Li.

These predictions are qualitatively consistent with observations of main-sequence stars in younger open clusters. Observations of stars in young clusters like the Pleiades (Soderblom et al. 1993) do confirm the general ZAMS Li–T_e relation

[3] Visiting Astronomer, Cerro Tololo Inter-American Observatory. CTIO is operated by AURA, Inc., under contract to the National Science Foundation.

[4] By "standard" we mean spherically symmetric models that ignore effects due to diffusion, rotation, mass loss, and magnetic fields.

resulting from pre-main-sequence evolution. However, stars in real clusters exhibit major departures from the theoretical expectations. A significant dispersion in the Li abundance is found at any given stellar mass or surface temperature, implying that factors beyond the star's basic structural parameters of mass, chemical composition, and age are relevant (King et al. 2000). An additional clue is posed by the observation that short-period, tidally locked binaries retain their high initial surface Li, an association that highlights rotation and/or stellar rotational history as additional factors (Deliyannis et al. 1994), in agreement with studies of both field stars (Randich et al. 1999; Chen et al. 2001; do Nascimento et al. 2003; Mallik et al. 2003; Jasniewicz et al. 2006) and clusters (Thorburn et al. 1993; Jones et al. 1999; Pasquini et al. 2004).

Among older open clusters, depletion of Li in low-mass stars as a function of stellar mass exceeds SSET predictions by amounts that grow increasingly disparate with age. At ages between 0.1 and 0.2 Gyr, a feature strikingly at odds with SSET begins to appear in plots of Li abundance versus stellar surface temperature or mass (Steinhauer & Deliyannis 2004). By the age of the Hyades (0.65 Gyr), stars with surface temperatures of 6600 ± 200 K, consistent with main-sequence masses near 1.4 $M_{\odot}$, show abrupt depletions in Li of up to 2 orders of magnitude, defining the Li or Boesgaard–Tripicco dip (Boesgaard & Tripicco 1986a). Such stars would not be expected to have convective envelopes; no obvious physical mechanism exists to put the surface layer in contact with the hotter, deeper layers. As emphasized by the many papers evaluating the properties relevant to this distinct feature (Pasquini et al. 2001, 2004; Chen et al. 2001; Boesgaard & King 2002; Mallik et al. 2003; Steinhauer & Deliyannis 2004), mapping the depth of the dip and its range in temperature and mass as a function of metallicity and age is critical to any attempt to decipher the underlying physical mechanism that produces it (Charbonnel & Talon 2005). Moreover, among clusters in the 3–5 Gyr range, the stars leaving the main sequence for the subgiant and giant branch emerge from the Li-dip with inherently lower Li that should be driven even lower by post-main-sequence evolution. Discovery of any evolved stars with measurable Li in clusters of this age range should be a clear indicator of anomalous evolution, mass transfer, and/or deep mixing of newly processed Li to the surface of stars on the giant branch (Balachandran 1995; Pasquini et al. 2001, 2004; Anthony-Twarog & Twarog 2004). Finally, the common age of cluster dwarfs offers the opportunity of defining reliably the time evolution of the Li depletion among the cooler stars beyond the Li-dip if significant samples with sufficient spectroscopic accuracy can be compiled over the age range of interest (Sestito & Randich 2005; Randich et al. 2006; Prisinzano & Randich 2007).

The focus of this investigation is the intermediate-age open cluster, NGC 3680. It was selected as a prelude to the analysis of a significantly more challenging but exceptional cluster, NGC 6253, for several reasons. As discussed in more detail in Section 3.3, some Li data for NGC 3680 stars from the turnoff through the giant branch do exist (Pasquini et al. 2001, hereafter PRP), though the sample at and below the turnoff is by no means complete; we hoped to broaden the characterization of the Li-dip profile by expanding the sample with comparably high signal-to-noise (S/N) spectra. At the same time, we wanted adequate overlap with previous work, not just so that conclusions might be strengthened by combined results for common stars in NGC 3680 but also to assist in validating our results for NGC 6253, based on spectra obtained with the same equipment and similarly reduced. Third, while photometric metallicity estimates are available for the turnoff stars and giants, as well as moderate-dispersion spectroscopic abundances for a few giants, metal abundances based on high-dispersion spectroscopy have been obtained for only a few cluster giants (Pasquini et al. 2001; Smiljanic et al. 2009; Santos et al. 2009) and two dwarfs (Pace et al. 2008; Santos et al. 2009), one of which might not be a member. Obtaining sufficiently high S/N spectra for NGC 3680's dwarf stars does not present an insuperable challenge, but the task is complicated by the severe paucity of single dwarfs in the cluster.

Broader astrophysical circumstances make NGC 3680 an intriguing target for observation. It is one of a trio of well-studied clusters of similar age: NGC 752 is closer than NGC 3680 but of comparable metallicity, while IC 4651 is more richly populated, more distant, and definitely more metal-rich than either cluster, as confirmed by both photometry (Anthony-Twarog & Twarog 1987, 2000; Nissen 1988; Meibom et al. 2002) and spectroscopy (Pasquini et al. 2004; Carretta et al. 2004; Pace et al. 2008). However, the modest metallicity range of ∼0.3 dex among the trio brackets the range occupied by the large majority of open clusters of any age within 1.5 kpc of the Sun (Twarog et al. 1997). Along with NGC 752 (Twarog 1983; Daniel et al. 1994), the color–magnitude diagram (CMD) of NGC 3680 exhibits a *bimodal* main sequence (Nissen 1988; Anthony-Twarog et al. 1989), i.e., a secondary sequence displaced to the red of the comparably populated main sequence, the byproduct of a rich binary population (Daniel et al. 1994; Nordström et al. 1997). Having collated photometry, proper motions, and radial velocities, Nordström et al. (1997) derived a binary fraction of 57% among ∼100 members of NGC 3680 with complete data.

NGC 3680, like IC 4651 and NGC 752, appears to have a poor to modest population below 1 $M_{\odot}$ (Anthony-Twarog et al. 1991; Hawley et al. 1999). Based on the extant stellar population, Nordström et al. (1997) estimate that the cluster mass might have been 10 times greater and the stellar population 30 times more numerous before its apparent evaporation.

The intermediate age of ∼1.7 Gyr for the three clusters places their turnoff stars squarely in the region of the Li-dip, but young enough that stars higher in mass than the dip should still be present near the turnoff region. The turnoff morphology also implies a turnoff mass that simultaneously corresponds to the mass for which convective core overshoot should play a conspicuous role (Mazzei & Pigatto 1988; Anthony-Twarog et al. 1989; Andersen et al. 1990; Daniel et al. 1994; Kozhurina-Platais et al. 1997). Confirmation of these characteristics has been based on exquisite information about proper-motion and radial-velocity memberships and binarity (Kozhurina-Platais et al. 1995; Mermilliod et al. 1995; Nordström et al. 1996). Once the numerous binaries are identified and removed from the CMD, the location of the single-star main sequence most resembles stellar models incorporating significant convective overshoot (Nordström et al. 1997).

The layout of the remainder of the paper is as follows: Section 2 details the spectroscopic observations and their reduction to produce radial velocities used in conjunction with proper motions to identify cluster members. Section 3 presents the fundamental parameters that play a role in the analysis of the spectra, as well as the derivation and interpretation of the abundances. Section 4 discusses the Li abundance pattern in NGC 3680, NGC 752, IC 4651, the Hyades, and Praesepe. The composite structure of the Li-dip and its possible evolution are

revisited in Section 5, and our conclusions are summarized in Section 6.

2. SPECTROSCOPIC DATA

2.1. Observations and Reductions

Spectra of 71 stars in NGC 3680 were obtained at the Cerro Tololo Inter-American Observatory Blanco 4 m telescope using the Hydra multi-object spectrograph. Three exposures for each of the two fiber-position configurations were obtained on 2005 July 18 and 19. One fiber configuration emphasized stars above the turnoff for a total exposure of 1 hr; the second reached further down the main sequence with a total exposure of 4 hr. Hydra was used in echelle mode; operating at relatively low order (8, in our case), dedicated filters select and pass the desired spectral region (filter 6 for our purposes). Our spectra were characterized by a dispersion of 0.15 Å per pixel in the range 6520 Å to 6810 Å with S/N per pixel that ranged from ∼160 to 20. Measured widths for calibration lamp lines imply a spectral resolution of 15,000 in the region near 6700 Å.

The numbering system of the proper-motion study by Kozhurina-Platais et al. (1995) (hereafter KGP) is one of the larger sets; it will be used in the discussions of our own data. All exposures for star KGP 1396 were severely compromised by placement of the spectra on a region of the chip affected by a filter defect, so no further discussion of results for this star based on our data will be included. Processing of the data and calibration frames was completed at Indiana University and the University of Kansas using standard programs within IRAF. For clarity, all quoted uncertainties refer to the standard deviation unless explicitly noted otherwise.

2.2. Radial Velocities

Radial-velocity and rotational-velocity estimates were derived for 70 stars in our program utilizing the Fourier transform, cross-correlation facility, FXCOR, in IRAF. Program stars are compared to stellar templates of similar temperature, in this case over the wavelength range from 6575 Å to 6790 Å including Hα, as well as a narrower region in the vicinity of Hα alone. A comparison of the results from these two internal measures demonstrates that, if two stars with significant discrepancies are excluded from the comparison (one is very cool, the other has very low S/N), the average difference in the radial-velocity determinations, in the sense (full spectrum—Hα), is -1.27 ± 2.9 km s^{-1}. The radial velocity for KGP 802 that appears in Table 1 is based on the Hα region alone; radial velocities for all other stars are based upon the full spectrum.

To refer the derived radial velocities to an absolute scale, two options exist. First, two radial-velocity standards were observed on each of the nights for the CTIO Hydra runs, HR 9014 and HR 9032. A comparison of our determinations with the values from the General Catalog of Radial Velocities (Wilson 1953) suggests that our velocities are too large by 1.1 ± 2.1 km s^{-1}. Second, we can also compare our radial velocities for 18 stars in common with Nordström et al. (1996) and three stars in common with Mermilliod et al. (1995). With known or suspected spectroscopic binaries excluded from the comparison, the average velocity difference, in the sense (N96—this study), is -0.45 ± 1.66 km s^{-1}, indicating that our radial velocities are consistent with Nordström et al. (1996) within the errors. A similar comparison to three apparently single-star red giants in common with the survey of Mermilliod et al. (1995) produces a velocity difference, in the sense (M95—this study), of -0.75 ± 0.53 km s^{-1}. We elected not to correct our radial velocity values based on these fairly noisy comparisons; additional discussion in the following session will suggest that our radial velocity values are larger than previous results by 0.4 km s^{-1}.

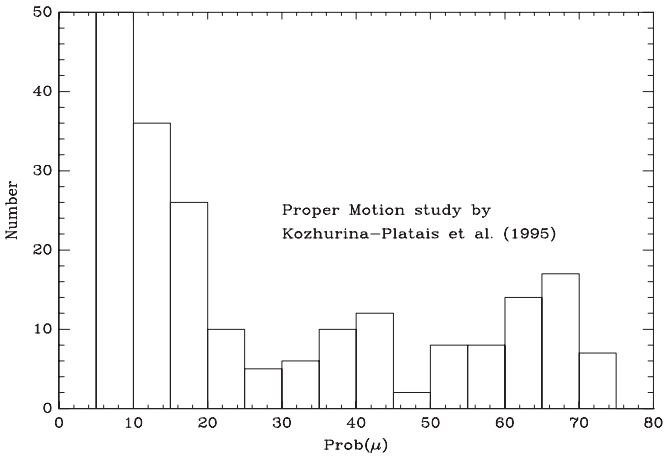

Figure 1. Proper-motion probability distribution for stars identified as most likely to be potential members of NGC 3680.

2.3. Cluster Membership

Radial-velocity studies by Mermilliod et al. (1995) and Nordström et al. (1996) established membership credentials for 15 red giants and over 100 red giant and dwarf stars, respectively, followed by an analysis of the cluster's evolutionary history (Nordström et al. 1997). A nearly parallel study by Kozhurina-Platais et al. (1997) followed similar lines. The proper-motion study by Kozhurina-Platais et al. (1995) yields membership probabilities for 2711 stars. By themselves, the proper-motion measures do not discriminate cleanly between cluster members and field stars for NGC 3680. This point is illustrated in Figure 1, a histogram of the number of stars as a function of proper-motion probability for the 391 stars described by Kozhurina-Platais et al. (1995) as "the most probable cluster members." From this figure alone, it is difficult to find a sharp distinction between members and non-members, except to conclude that stars with $P(\mu) \leqslant 10\%$ to 20% are unlikely to be members. Kozhurina-Platais et al. (1995), as well as Nordström et al. (1996, 1997), combine information from radial velocities and proper motions to establish more comprehensive membership criteria. In the discussion of memberships for our candidate stars that follows, we will employ the proper-motion-based probabilities of Kozhurina-Platais et al. (1995) and radial velocities determined from our spectra.

Figure 2 shows our radial velocities, along with proper-motion-based membership probabilities for our 70 program stars, indicating a cluster mean radial velocity near 2 km s^{-1} and illustrating the eventual criteria for cluster membership. Whether or not binaries are included, the median radial velocity for stars with $P(\mu) \geqslant 20\%$ is 1.6 km s^{-1}. The average radial velocity for 24 stars with proper-motion membership probability $P \geqslant 20\%$ that are not known or suspected spectroscopic binaries, is 1.64 ± 1.22 km s^{-1}. If giants are excluded, the mean becomes 1.72 ± 1.22 km s^{-1}. The average radial velocity for the four single-star, red giant members (KGP 1175, 1374, 1461, and 1873) is 1.28 ± 0.56 km s^{-1}. As expected from the earlier discussion, our mean radial velocity from single member dwarfs is 0.45 km s^{-1} larger than that of Nordström et al. (1997), who

Table 1
Basic Data for Program Stars in NGC 3680

KGP	WEBDA	Eggen	V	$B-V$	$P(\mu)$	$V \sin i$	$\sigma_{\rm rot}$	$V_{\rm rad}$	$\sigma_{\rm rad}$	Comments
802	176		16.803	1.038	2	8.4	0.5	2.7	...	
803	177		14.754	0.608	15	13.5	2.5	−19.3	3.2	
833	183		15.520	0.773	5	13.4	0.5	−0.9	1.0	
873	190		15.255	0.708	4	4.1	0.1	4.5	0.6	
936	4028		12.665	0.443	65	30.8	0.9	1.1	1.2	
945	3004		15.585	0.797	17	17.3	0.6	−2.2	1.0	sb?
952	4081		12.371	0.488	71	14.3	0.4	1.9	0.9	SB1(N97)
979	4119		16.756	1.028	3	14.7	0.6	16.6	1.2	sb?
983	4021		14.952	0.648	37	16.1	0.4	3.2	0.7	
988	79	R	11.827	0.451	51	58.4	2.4	−5.0	3.1	w/sb?
1008	3095		12.241	0.501	64	40.6	1.8	1.8	2.3	w/sb?
1035	1	1	11.894	0.446	60	39.5	1.6	−0.3	1.9	SB2(N97)
1050	70	I	14.621	0.591	37	10.6	0.3	1.6	0.7	
1083	4	4	12.923	0.476	61	24.1	0.6	0.6	0.9	
1097	3064		14.136	0.600	52	22.5	0.8	18.0	1.1	SB? (KP97);sb?
1119	4073		16.333	0.926	3	7.6	0.2	−16.2	0.8	
1123	4132		15.650	0.813	18	8.3	0.2	79.9	0.6	
1138	72	K	12.695	0.434	53	46.5	2.4	6.2	3.0	w/sb?
1168	14	14	12.354	0.444	65	30.0	1.2	−0.8	1.5	SB2(N97)
1175	13	13	10.822	1.158	70	16.8	0.3	1.4	0.5	
1192	15	15	12.501	0.481	69	18.0	0.4	1.3	0.7	
1194	5	5	12.845	0.430	67	12.0	0.3	3.0	0.7	SB1(N97)
1197	16	16	13.321	0.511	63	11.0	0.4	50.8	0.9	SB2(N97)
1202	4038		16.350	0.797	5	3.9	0.2	−15.4	0.9	
1207	6	6	12.475	0.508	65	22.9	0.5	2.8	0.8	
1208	19	19	12.364	0.494	70	45.4	3.9	3.2	4.8	w/sb?
1218	222		13.943	0.485	54	16.4	0.4	1.4	0.7	
1243	12	12	15.041	0.705		12.1	0.2	13.6	0.6	
1261	20	20	10.139	1.007	59	16.8	0.2	0.8	0.4	SB2(N97,M95)
1274	227		14.472	0.554	51	6.3	0.2	1.9	0.6	
1286	11	11	10.920	1.049	61	15.6	0.3	−0.9	0.6	SB1(N97,M95)
1304	80	21A	14.762	0.724	2	21.5	1.1	2.3	1.7	SB2(N97)
1319	10	10	12.827	0.434	71	40.6	1.5	−0.2	1.7	w/sb?
1324	39	39	12.428	0.510	66	11.9	0.3	2.0	0.7	SB? (KP97)
1331	81	25A	13.655	0.476	59	25.7	0.8	2.4	1.1	
1347	38	38	12.450	0.490	65	45.7	2.2	2.0	2.7	SB1(N97)
1350	33	33	11.910	0.487	66	15.0	0.4	−0.6	0.8	SB1(N97)
1352	3055		15.679	0.781	2	11.6	0.5	12.7	1.1	
1355	3081		16.582	0.866	5	10.6	0.5	11.2	1.3	
1365	3001		12.801	0.438	70	8.4	0.2	−0.7	0.7	
1374	26	26	10.952	1.127	62	17.5	0.3	0.7	0.5	
1376	35	35	13.077	0.478	68	11.0	0.2	1.6	0.5	
1379	34	34	10.623	0.895	63	19.6	0.4	4.3	0.6	PhotBin(M95;AHTC)
1395	37	37	13.030	0.433	53	22.2	0.7	1.8	1.0	
1404	27	27	10.770	1.134	71	16.0	0.3	2.2	0.6	SB1O(M95,N97,M07)
1405	31	31	13.135	0.456	69	21.6	0.6	0.4	0.8	SB1(N97)
1410A	240B		12.424	0.437	...	60.3	3.1	1.1	4.1	SB?(KP97); w/sb?
1446	2058		15.801	0.795	16	10.6	0.4	51.2	0.9	
1454	32	32	12.917	0.478	66	21.2	0.5	2.0	0.8	SB1(N97)
1461	41	41	10.930	1.121	23	16.6	0.3	1.0	0.5	
1469	44	44	10.002	1.235	67	17.2	0.3	1.2	0.6	SB? (KP97)
1506	42	42	12.977	0.441	62	51.4	2.8	−2.7	3.7	sb?
1507	46	46	13.358	0.452	60	16.0	0.4	2.0	0.7	
1510	43	43	12.552	0.448	68	30.6	1.6	2.6	1.9	PhotBin(ATTS)
1522	45	45	12.034	0.504	67	30.6	1.1	1.2	1.4	
1524	82	46A	13.498	0.485	49	29.3	0.8	1.4	1.0	SB?(KP97)
1534	1085		14.309	0.565	42	5.6	0.1	2.6	0.6	
1554	1124		14.285	0.537	51	11.0	0.3	2.9	0.8	
1575	2089		14.464	0.586	1	5.1	0.2	−29.4	0.7	
1588	2005		16.079	0.852	8	6.6	0.3	−1.9	1.1	
1610	2017		16.752	0.946	3	6.2	0.2	3.4	1.0	
1612	2084		15.404	0.712	13	13.5	0.3	−0.1	0.5	
1624	2062		13.634	0.467	61	18.3	0.4	−1.8	0.7	SB1(N97)
1627	2109		15.811	0.867	14	8.2	0.2	8.4	0.7	
1638	58	58	12.891	0.434	58	21.1	0.8	22.7	1.1	SB1(N97)

Table 1
(Continued)

KGP	WEBDA	Eggen	V	$B-V$	$P(\mu)$	$V \sin i$	$\sigma_{\rm rot}$	$V_{\rm rad}$	$\sigma_{\rm rad}$	Comments
1649	2110		12.571	0.456	57	32.4	1.2	−0.4	1.4	
1690	51	51	(14.57)	(0.59)	10	13.9	0.5	4.4	0.9	
1722	1019		15.087	0.717	33	17.5	0.3	0.2	0.6	
1815	1076		15.241	0.711	6	11.2	0.3	−12.9	0.6	
1873	53	53	10.859	1.120	69	18.0	0.3	2.0	0.7	

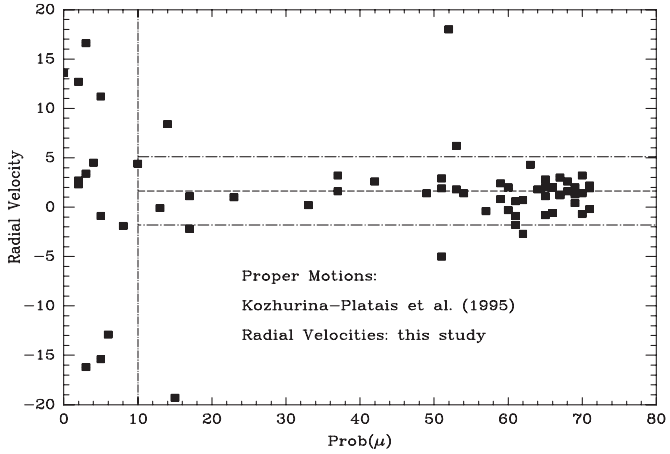

Figure 2. Radial velocities for the stars in the current study as a function of the proper-motion probability. The dashed horizontal line defines the cluster mean velocity from the probable dwarf members, while the horizontal dash-dotted lines define the radial-velocity limits for probable single-star cluster members, between −1.8 and 5.1 km s^{-1}.

find a mean of 1.27 km s^{-1} from dwarf members. Our average based on red giants alone is similarly 0.41 km s^{-1} larger than the value 0.87 km s^{-1} found by Mermilliod et al. (1995) from giant members. Nordström et al. (1997) comment on the difference between the average radial velocity of the main sequence and giant stars, and conclude that it is consistent with an expectation based on different surface gravities for the two classes of stars; we also find a difference of ∼0.4 km s^{-1} between the dwarfs and giants, but the significance of this difference appears to be only marginal in our case. Nordström et al. (1997) estimate the internal velocity dispersion from dwarf stars as 0.65 km s^{-1}; using an estimate of our internal accuracy of ±0.9 km s^{-1} leads to a velocity dispersion of 0.8 km s^{-1}.

Entries in Table 1 include the more common identifications: KGP, as used by SIMBAD, referring to Kozhurina-Platais et al. (1995); the well-known Eggen numbers (Eggen 1969); WEBDA numbers, which use Eggen numbers for the brighter stars and refer to other surveys for the fainter stars. Photometric V magnitudes and $B-V$ colors are taken from the collated and merged values as described by Anthony-Twarog & Twarog (2004) (hereafter ATT). Estimates of rotational velocity and radial velocity follow, each with error estimates from FXCOR in IRAF. The final column summarizes information about binarity. Comments about binary status are as specific as possible, including notations "SB?" referring to the analysis of radial-velocity errors by Kozhurina-Platais et al. (1997) that suggest binary status and, similarly, "w/sb?" indicating that our spectra suggest unusually wide and/or doubled lines in the instrumental spectra. Stars with proper-motion probabilities and radial velocities within the bounds illustrated in Figure 2, between −1.8 and 5.1 km s^{-1}, are considered members; note that while using a modest radial-velocity range to constrain membership, we have extended the proper-motion probability limit to 10%.

3. CLUSTER PROPERTIES—NGC 3680

3.1. Age and Distance Estimates

ATT collated and mapped Strömgren $b-y$ colors from four other surveys to their own photometry in NGC 3680, then mapped the magnitudes and colors to the broad-band photometric system of Kozhurina-Platais et al. (1997). These are the photometric values we will use in the analyses of our spectroscopic data below. ATT presented independent determinations of the interdependent quantities of foreground reddening and overall metal abundance for NGC 3680, as well as extensive reviews of earlier determinations of both; the reader is referred to this discussion for details. In summary, NGC 3680 was found to have $E(B-V) = 0.058 \pm 0.003$ (sem), well within the range bounded by the UBV-based estimate of 0.04 by Eggen (1969) and the high-end determination of 0.10 from DDO photometry of the giants (Clariá & Lapasset 1983; Twarog et al. 1997).

Photometric metallicity estimates from the intermediate-band m_1 and hk indices led to a value of [Fe/H] = −0.14 ± 0.03 dex (sem), lower than the earlier estimates of +0.09 to +0.11 (Anthony-Twarog et al. 1989; Nordström et al. 1997; Bruntt et al. 1999) tied to the photometry of Nissen (1988). The lower metallicity removed the apparent discrepancy between the photometric dwarf abundances and those of the giants defined by DDO photometry, moderate-dispersion spectroscopy (Twarog et al. 1997), and high-dispersion spectroscopy (PRP). Mindful that spectroscopic analyses are necessarily tied to stellar parameters obtained assuming an a priori metallicity estimate, we adopted an initial value of [Fe/H] = −0.14 based upon the photometric results of ATT but iteratively settled on a value of [Fe/H] = −0.08. The rationale behind this choice is discussed in Sections 3.4–3.6.

With reddening and abundance estimates in hand, a comparison of the homogeneous photometry to appropriate isochrones constrains the cluster age and distance, while providing measures of the individual stellar surface gravities. The CMD based on the composite BV photometric values (ATT) for 63 probable members, selected using the joint proper-motion (Kozhurina-Platais et al. 1995) and radial-velocity criteria discussed in Section 2.3 from the stars observed for this investigation and those of PRP, is shown in Figure 3, with open symbols denoting the 22 stars for which some binary status is known or suspected. Triangles are stars for which only the Li data of PRP are available. While the photometric data set is not substantively different from that used by ATT, the isochrones and interpolation software for specific ages and abundances adopted for the present discussion are those of Y^2 (http://www.astro.yale.edu/demarque/yyiso.html; Yi et al. 2003; Demarque et al. 2004), rather than the updated Padova isochrones (http://stev.oapd.inaf.it/cgi-bin/cmd).

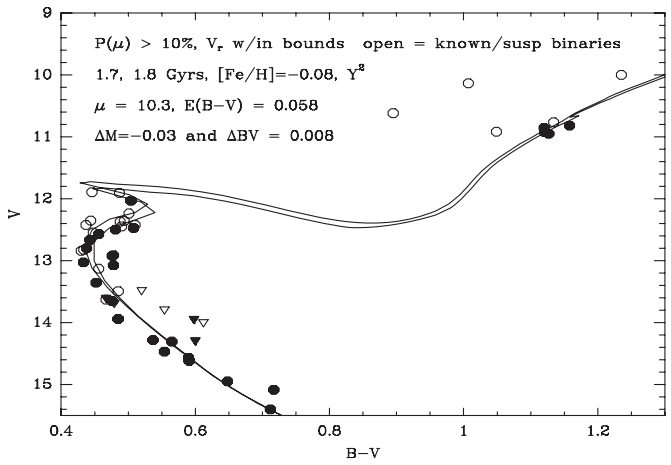

Figure 3. CMD for stars observed in the present study, excluding probable non-members. Filled circles are likely cluster members, while open circles identify members that are suspected of being binaries. Triangles denote stars observed by PRP, with binaries similarly denoted by open symbols. Superposed are Y^2 isochrones of appropriate metallicity with ages of 1.7 Gyr and 1.8 Gyr, adjusted for the reddening and apparent distance modulus of NGC 3680.

The latter models (Marigo et al. 2008) are substantially the same as the Girardi et al. (2002) models used in ATT and require similar offsets of +0.01 mag and −0.023 mag, respectively, to the M_V and $B-V$ color scales to bring a 1 $M_\odot$ star of age 4.6 Gyr (Bahcall et al. 1995; Houdek & Gough 2008) into alignment with our consistently adopted values of 4.84 and 0.65 for the solar M_V and $(B-V)$ color. The comparable shifts for the Y^2 set are −0.03 and +0.008, respectively. The Padova solar isochrones are defined using the $Z = 0.019$ set as the solar composition, while Y^2 define solar as $(Y,Z) = (0.266, 0.0181)$. The switch in isochrone sets allowed a comparison with earlier work to get an indication of how sensitive the conclusions are to the specific models adopted, but was explicitly done because the Y^2 isochrones generate masses for the stars in the Li-dip that are more internally consistent with age, a point we will return to in Sections 4 and 5. For $Z = 0.0152$ ([Fe/H] = −0.08), Y^2 isochrones with ages of 1.7 Gyr and 1.8 Gyr are displayed in Figure 3, adjusted for the adopted reddening of $E(B-V) = 0.058$ and an apparent distance modulus of $(m-M) = 10.3$. The age and apparent distance modulus are in good agreement with those discussed in ATT (1.85 Gyr, 10.2); the revised Padova isochrones yield 1.85 Gyr and $(m-M) = 10.2$, while supplying a slightly better match to the shape of the turnoff below the hook.

Note in Figure 3 that the stars traditionally identified as the clump have the predicted luminosity for He-core-burning stars in this phase but overlap the colors of the first-ascent giant branch. Moreover, the luminosity of the majority of the stars also is consistent with the location of the red giant bump, where first-ascent giants temporarily reverse their evolution up the giant branch when the H-burning shell crosses the discontinuity in composition created by the deep limit of the convective atmosphere as the star ascends the giant branch.

The solid agreement between observation and theory in Figure 3 boosts confidence in the derived stellar parameters needed for the spectroscopic analysis that can be deduced differentially from the CMD. As exemplified by the Padova comparison, however, even assuming a fixed reddening and metallicity, adoption of a different set of isochrones based upon alternate models could result in slightly different age, distance, surface gravity, and mass estimates for the individual stars. From the detailed discussion in ATT, the spread in $(m-M)$ found in the recent literature for NGC 3680 is a byproduct of the combined variation in the derived [Fe/H], the adopted reddening, and the choice of stellar isochrones, as exemplified by the values of $(m-M) = 10.45$ to 10.65 derived by Nordström et al. (1997) and Kozhurina-Platais et al. (1997) adopting [Fe/H] much closer to Hyades metallicity for the cluster, as well as alternate sets of isochrones.

3.2. Cluster Metallicity—Li

SPLOT, part of the one-dimensional spectrum analysis suite in IRAF, was used to measure equivalent widths of the line blend incorporating the Li-doublet at 6707.8 Å and the Fe I line at 6707.45 Å; the EW measures are summarized in Table 2, along with the estimated S/N for each spectrum. S/N per pixel estimates were based on the modal statistics of the spectra in a "relatively" line-free region between 6615 Å and 6625 Å. Li measurements were not possible in some stars: either the line was too weak to be measured or the spectrum was distorted in a way which made measurement implausible. Of the eight stars in the latter category, three have S/N per pixel below 30 (KGP 802, 803, and 1610), while the others (KGP 979, 988, 1347, 1410A, and 1506) are known or suspected spectroscopic binaries whose multiple components confused the Li-line region beyond reclamation.

The largest set of Li EW measurements and abundance estimates for NGC 3680 is that of PRP, offering abundances for 26 stars, including two suspected non-members, and expanding on an earlier discussion of four approximately solar-type stars by Randich et al. (2000). While the larger sample of PRP will supply the comparison of choice for our measurements, the discrepancy between the published equivalent widths from the same authors for the four stars based upon the same spectra highlights the challenge of comparing results from different groups using different spectra. The Li EW estimates for the four cool, main-sequence stars in Randich et al. (2000) are 8 ± 2 mÅ smaller than those found in PRP, leading to an average Li abundance that is 0.07 ± 0.01 dex higher in the more recent study. Although PRP discounted the memberships of KGP 1405 and KGP 1365, we include them as possible members. It also seems probable that PRP followed an incorrect identification by Nordström et al. (1996) of their star 3001 as KGP 1353; it appears that this star is in fact KGP 1365, with a high probability of membership according to Kozhurina-Platais et al. (1997). Eighteen stars from PRP overlap with the present study, but only 13 have measurable Li lines in both. For these 13 stars, the equivalent widths in PRP are larger by 4.3 ± 11.1 mÅ, essentially midway between the values of Randich et al. (2000) and PRP, suggesting that our measurements are on the same system within the errors.

Following Steinhauer & Deliyannis (2004), we exploit the estimate for the metal abundance of the cluster stars to predict and remove the contribution of the Fe I line to the EW measurement for Li. The corrected equivalent width for the 6708 Å line, listed in Table 2 as EW′, along with the measured line width, temperature, and S/N estimates for each star provide input to a grid of abundance estimates developed by Steinhauer (2003) from MOOG model atmospheres and employed by Steinhauer & Deliyannis (2004). For three stars outside the temperature range of the model grid, MOOG was used interactively to estimate the Li abundance for the adopted values of temperature and surface gravity by comparing synthesized to observed spectra. A measured line may produce, at best, an upper limit for the

Table 2
Lithium EW and Abundance Data for Program Stars in NGC 3680

KGP	Temp.	EW	EW′	σ_{EW}	A(Li)	σ_A	S/N per pixel	FWHM
Abundances from Detected Lithium Lines								
873	5659	76.4	69.9	11.7	2.34	0.10	42	0.53
936	6707	94.3	94.3	5.3	3.41	0.04	139	1.18
952	6515	108.9	108.0	7.1	3.37	0.05	77	0.66
983	5879	36.9	32.0	8.0	2.13	0.13	46	0.30
1035	6694	84.1	84.1	5.4	3.33	0.04	132	1.10
1050	6098	59.7	56.2	9.2	2.63	0.09	58	0.62
1097	6063	70.4	66.7	6.6	2.70	0.06	84	0.68
1138	6746	65.6	65.6	7.0	3.22	0.06	110	1.30
1168	6703	54	54.0	6.3	3.08	0.06	107	0.99
1175	4606	86.2	71.2	3.2	1.02	0.03	163	0.58
1192	6545	50.8	50.1	7.8	2.93	0.09	68	0.62
1194	6763	46.1	46.1	3.5	3.03	0.04	133	0.47
1197	6419	46.1	44.7	4.8	2.77	0.06	112	0.64
1207	6432	120.7	119.3	7.4	3.38	0.05	89	0.95
1261	4892	44.4	32.0	2.5	0.98	0.04	209	0.59
1274	6244	51.6	49.1	6.6	2.68	0.07	66	0.42
1286	4808	34.7	21.6	2.2	0.50	0.10	233	0.59
1319	6746	70.6	70.6	5.4	3.26	0.05	124	0.99
1324	6424	74.6	73.2	9.6	3.05	0.08	77	1.20
1350	6519	28.7	27.9	6.7	2.61	0.12	69	0.47
1352	5404	104.8	96.5	24.9	2.26	0.17	21	0.60
1365	6729	62.8	62.8	4.1	3.18	0.04	138	0.69
1374	4662	92.2	77.8	10.2	1.15	0.08	56	0.72
1376	6557	18.1	17.5	4.3	2.41	0.12	114	0.52
1404	4649	85.7	71.2	2.3	1.09	0.02	225	0.61
1405	6651	50.3	50.2	5.1	3.00	0.05	113	0.72
1454	6557	42.6	42.0	4.4	2.84	0.06	136	0.80
1461	4672	35.6	21.3	0.0	0.40	0.10	225	0.51
1522	6448	47.3	46.0	8.6	2.81	0.10	74	0.88
1534	6200	77.8	75.0	7.4	2.88	0.06	72	0.62
1612	5644	44.5	37.9	11.1	1.99	0.17	44	0.52
1638	6746	35.4	35.4	4.5	2.89	0.06	109	0.52
1649	6651	24.4	24.3	4.6	2.64	0.09	128	0.76
1690	5857	66.1	61.0	9.9	2.46	0.09	48	0.50
1873	4674	90.5	76.2	3.3	1.16	0.03	167	0.65
Upper Limit Lithium Abundances								
1008	6461	20			2.49		55	0.42
1083	6566	7.7			2.06		156	0.39
1123	5297	9			1.16		49	0.21
1208	6482	8			2.31		76	0.36
1218	6528	7			2.19		80	0.20
1243	5670	7.8			1.77		49	0.34
1304	5602	<11			1.88		46	
1331	6566	<7			2.54		70	
1355	5126	36.2			1.60		25	0.50
1379	5036	25.4			0.82		90	0.67
1395	6750	<5			2.48		104	
1446	5357	9			1.52		39	0.34
1469	4475	35.4			0.00		315	0.53
1507	6668	10			2.43		82	0.39
1510	6729	5			2.42		67	0.20
1554	6313	25.8			2.38		62	0.54
1575	6117	<9			2.26		59	
1627	5123	4			1.13		25	0.10
1722	5627	19.6			1.67		60	0.43
1815	5648	8			1.79		39	0.26

Li abundance if EW′ is no larger than three times the estimated error, as formulated by Deliyannis et al. (1993); stars meeting this criterion are listed separately in Table 2.

A key component in abundance estimation is the scheme by which temperatures are derived for stars. For our analysis, temperatures for the unevolved stars have been based exclusively upon the reddening-corrected $B-V$ colors, transformed to the temperature plane using the polynomial relation of Deliyannis et al. (2002):

$$T_e = 8575 - 5222.7(B-V)_0 + 1380.92(B-V)_0^2 + 701.7(B-V)([\mathrm{Fe/H}] - [\mathrm{Fe/H}]_{\mathrm{Hyades}}).$$

For our analysis, [Fe/H] for the Hyades was set at +0.15, while the abundance for NGC 3680 was assumed to be −0.08. For [Fe/H] = 0.0, at a solar T_e of 5770 K, the implied $B-V$ color is 0.63, slightly bluer than our normally adopted value of 0.65 for CMD fits to isochrones. If we demand that the temperature scale match the redder color, it is equivalent to shifting the scale upward by ∼65 K.

Since the relation above is defined by dwarfs in the temperature range bracketing the Sun, it is not applicable to the giants in NGC 3680. For the evolved stars, we converted $(B-V)_0$ to T_e using the color–temperature relation of Ramírez & Meléndez (2005), an update of the dwarf and giant calibrations of Alonso et al. (1996, 1999). For comparison purposes, over the dwarf color range of interest, the Ramírez & Meléndez (2005) scale predicts temperatures systematically cooler by ∼25 K than the predicted values from the relation adopted above. Final derived values of T_e for each star can be found in the second column of Table 2. The derived Li abundances are presented in Table 2, with the stars separated according to whether the star had a measurable Li abundance or an upper limit as defined by the criterion described earlier.

3.3. Li—Comparison with Previous Work

PRP employed $B-V$ photometry (Nordström et al. 1996) to estimate temperatures for the dwarfs (Alonso et al. 1996) and giants (Alonso et al. 1999). From the 20 dwarfs and six giants discussed by PRP, the mean temperature differences, in the sense (PRP—this study), are −83 ± 63 K and +27 ± 57 K, consistent with PRP dwarf colors that are systematically redder by about 0.03 mag while the giants are bluer by 0.01 mag. Note that the comparison can be made for the entire sample because we have $B-V$ colors for every star analyzed by PRP, not just the overlap with this work. The offset flip between dwarfs and giants as well as the scatter are products of the lower precision $B-V$ colors adopted by PRP. Our colors are based upon a weighted average of a number of photoelectric and CCD studies transformed to a common system, resulting in typical uncertainties in the photometric colors at the 0.003–0.010 mag level.

To enable a more realistic assessment of the two abundance scales and provide some means of merging the two, we have adjusted the Li abundances of PRP to our $(B-V)$-based temperature scale using the prescription for the temperature dependence as supplied by PRP. For seven dwarfs with measurable Li in both studies, the mean residual, in the sense (PRP—this study) is −0.02 ± 0.14 dex. If the star with the largest discrepancy is dropped, the average for six stars is +0.01 ± 0.10 dex. The Li abundances for these seven dwarfs will be based upon the average of the two measures, without adjustment for an offset. For the four giants with measured Li, the mean residual is −0.11 ± 0.11 dex. This offset has been applied to the data of PRP and averaged with ours. In the following discussions of NGC 3680 as a representative of intermediate-age open clusters, the Li abundances of PRP for stars not observed in the current investigation will be used to augment the cluster sample, with the offsets based upon the dwarf and giant comparisons applied as needed.

Based upon multiple abundance reductions for our sample under different assumptions for the temperature scale, we find that a change in T_e of ±60 K will alter A(Li) by ±0.05 dex for the dwarf stars. For the giants, a comparable temperature change alters A(Li) by ±0.09 dex.

3.4. Cluster Metallicity—Fe, Ca, Si, Ni

The determination of the metal abundance of NGC 3680 began with the adoption of a list of cleanly measurable iron lines used in common with other cluster investigations by the authors from the Indiana University group. To these eight Fe lines we added six measurable lines of neutral Si, Ca, and Ni. Equivalent widths were measured using the IRAF routine SPLOT, then processed using the force-fit abundance routines in MOOG. These steps were replicated for 15 separate exposures of the solar spectrum obtained from our daytime sky exposures from the 2005 Hydra run, adopting an effective temperature of 5770 K, surface gravity of log $g = 4.40$ and a microturbulent velocity of 1.14 km s^{-1} for the Sun. Signal-to-noise ratios per pixel for each of these solar spectra ranged from 90 to 230. All resulting stellar abundances were differenced with respect to the generated solar abundances on a line-by-line basis.

MOOG provides abundances for each measured equivalent width consistent with an appropriately selected atmospheric model, so the choices of atmospheric parameters are critically important. The choices for temperature scales based on $(B-V)$ colors have been described earlier; gravities were determined by examining isochrones fitted to the observed CMD as shown in Figure 3. For composite systems, this will lead to slightly lower gravities than expected for a single star, but the change is too small to have a serious impact on the final abundance estimates. Microturbulent velocities for dwarf stars were computed from temperatures and surface gravities using the algorithm of Edvardsson et al. (1993).

Abundances for the giant stars, for which the Edvardsson et al. (1993) algorithm is not applicable, are considerably more sensitive to the choice of microturbulent velocity. As a starting point we considered the formula proposed by Carretta et al. (2004): $v_t = 1.5 - 0.13 \log g$, which yields v_t values between 1.16 km s^{-1} and 1.24 km s^{-1} for the eight giant stars in NGC 3680. However, based upon the standard technique of minimizing the trend between the residuals in [Fe/H] and the EW for the lines, PRP found significantly larger values of $v_t =$ 1.70 km s^{-1} for their coolest giant and 1.90 km s^{-1} to 1.95 km s^{-1} for the remaining five giants. Attempts to apply the Carretta et al. (2004) formula to our spectra also failed to achieve appropriate minimization of the slope between the residuals and the EW. A range in v_t was tested for each star until a satisfactory slope was achieved. The resulting trend of v_t with log g preserved the Carretta et al. (2004) gravity dependence of v_t but implied an intercept larger by 0.35 km s^{-1}, midway between PRP and Carretta et al. (2004).

Results for individual stars are presented in Table 3. For the giant stars, all eight Fe lines and the six additional metal lines were measurable in all eight stars. For the dwarf stars, from four to six iron lines were measurable in the chosen stars along with the 6717 Å line of Ca, the 6721 Å Si line, and the three Ni lines. The abundances for the dwarf stars exhibited no dependence on T_e, though the temperature range is modest. An examination of the abundances as a function of S/N, however, suggests that the most consistent dwarf abundances are obtained from the five dwarfs with the highest S/N spectra; these five stars are designated in Table 3 by KGP identification numbers in bold font. For reference, we note here that we have conformed with what is presumably a standard practice when combining separate measures of [A/H], namely constructing a simple mean of [A/H] values. It was anticipated that following this practice would facilitate comparison with other published work, but it cannot be

Table 3
Metal Abundance Data for Program Stars in NGC 3680

KGP	[Fe/H]	σ_{Fe}	N_{lines}	[Si/H]	[Ca/H]	[Ni/H]	σ_{Ni}
			Giants				
1175	−0.13	0.13	8	0.20	...	−0.15	0.04
1261	−0.18	0.11	8	0.00	...	−0.33	0.05
1286	−0.22	0.06	8	−0.16	...	−0.10	0.07
1374	−0.31	0.12	8	0.00	...	−0.21	0.20
1404	−0.10	0.13	8	0.13	...	−0.14	0.04
1461	−0.22	0.09	8	0.09	...	−0.21	0.06
1469	−0.14	0.16	8	0.17	...	−0.09	0.04
1873	−0.09	0.23	8	−0.02	...	−0.10	0.11
			Dwarfs				
952	0.00	0.22	6	0.02	−0.05	−0.08	0.26
1083	−0.09	0.22	6	−0.20	−0.32	−0.35	0.37
1194	−0.08	0.17	6	−0.13	−0.14	−0.11	0.15
1218	0.05	0.17	5	0.04	−0.02	0.00	0.32
1324	−0.06	0.15	6	0.04	−0.01	−0.17	0.27
1331	−0.25	0.07	4	−0.07	−0.31	−0.07	0.06
1365	−0.07	0.23	6	−0.16	−0.21	−0.14	0.19
1376	−0.03	0.24	6	−0.07	−0.18	−0.09	0.19
1395	−0.19	0.12	4	−0.14	−0.39	−0.22	0.10
1454	−0.10	0.12	6	−0.10	−0.24	−0.21	0.32
1507	−0.03	0.19	5	0.08	−0.06	0.08	0.11
1534	0.14	0.30	6	0.07	−0.13	0.01	0.20
1624	0.13	0.03	5	−0.22	−0.11	−0.16	0.09

Table 4
Abundance Data by Line for Program Stars in NGC 3680

λ	[A/H] Giants	σ	[A/H] Dwarfs	σ	N_{stars}
		Iron			
6581.2	−0.23	0.16			
6608.0	−0.25	0.11			
6609.1			−0.23	0.09	11
6678.0	−0.07	0.10	−0.20	0.13	13
6703.6	−0.12	0.13			
6725.4	−0.06	0.15			
6726.7	−0.15	0.13	−0.03	0.19	13
6733.2	−0.20	0.08	0.20	0.15	10
6750.2	−0.34	0.09	0.01	0.14	13
6752.7			0.08	0.10	11
		Calcium			
6717.7			−0.17	0.12	13
		Nickel			
6643.6	−0.14	0.11	−0.27	0.22	13
6767.8	−0.20	0.11	0.03	0.14	13
6772.3	−0.16	0.11	−0.11	0.16	13
		Silicon			
6721.8	0.05	0.12	−0.06	0.10	13

construed as a *correct* way to combine logarithmic values. The preferred approach (taking the logarithm of averaged numerical abundances) yields abundances that are typically larger by amounts that reflect the scatter among individual values.

3.5. Metallicity—Giants

The mean [Fe/H] for eight giants in Table 3 is -0.17 ± 0.07, with comparable values for Si of $+0.05 \pm 0.12$, based on one line, and -0.17 ± 0.08 for the three lines of Ni. A weighted average for [Fe/H] gives -0.18 ± 0.07. While the balance of the measures clearly favors a subsolar abundance for NGC 3680, it leads to the obvious question of the zero point of the metallicity scale since the solar spectra and their analyses are distinctly removed from the much cooler and more luminous giants. To test our [Fe/H] estimate, we turn first to the six giants analyzed by PRP, five of which have abundances in our survey. PRP obtained [Fe/H] $= -0.26 \pm 0.11$ from six giants. The first step in the comparison is to correct for the differences in temperature caused by PRP's use of less precise photometry, a smaller reddening, and a different $B-V$ calibration. This adjustment produces only a modest decrease in the PRP mean value to [Fe/H] $= -0.28$, while reducing the scatter to ± 0.08 dex. The truly significant adjustment comes from the difference in the adopted v_t. For the five stars common to the two samples, if we had adopted the microturbulence values used by PRP, the mean [Fe/H] would shift by -0.13 ± 0.05 dex. This is exactly the difference and the scatter one gets by taking the average residual for the five giants after placing the abundances on the same temperature scale. We have shifted PRP's data for the six giants by +0.13 dex and averaged our values with theirs for the five stars in common to derive a mean [Fe/H] $= -0.15 \pm 0.08$ from nine giants. The slightly higher value of [Fe/H] comes from the inclusion of KGP 1379 (E34), which has the highest abundance of all the giants. We opted not to analyze this star since its composite color would likely distort any temperature estimate. As one might expect, if this star is dropped, the mean [Fe/H] of the remaining eight giants becomes -0.17 ± 0.06.

Two high-resolution spectroscopic investigations of giants in NGC 3680 have been published recently. Smiljanic et al. (2009) discussed the giant KGP 1175 (EG13), for which they derive [Fe/H] $= +0.04 \pm 0.11$ (sd). In spite of their note to the contrary, this star is one of the five studied by PRP that overlaps with the current investigation. For their analysis, the stellar parameters $T_e = 4660$ K, log $g = 2.6$, and $v_t = 1.3$ km s^{-1} were derived purely from the requirements of internal consistency among the line abundances with EW, ionization state, and excitation potential. Our temperature for this star is 4606 K, while PRP get 4668 K. Adjusting to our scale would lower the [Fe/H] to approximately −0.01. Our log g is 2.56, so no correction is required, leaving a difference of 0.12 dex between their estimate and ours for this star. If our derived v_t of 1.56 km s^{-1} is reduced to 1.30 km s^{-1}, our [Fe/H] is shifted by 0.11 dex, accounting for the remainder of the difference.

The second paper (Santos et al. 2009) details spectroscopy of three single-star giants, 1175, 1374, and 1461, analyzed using two different line lists, with the stellar parameters set spectroscopically. The two line lists generate different combinations of the stellar parameters for the same star, but the systematic offset between the abundances for the three giants is only 0.02 dex, even though the temperature scales differ by 127 K. The temperature shift appears to compensate in part for the systematic change in v_t, which drops by an average of 0.05 km s^{-1} for the lower T_e scale. As an example of the size of the effects we are discussing, for KGP 1175 on the cooler temperature scale, Santos et al. (2009) find (4657 K, 2.68 dex, 1.38 km s^{-1}) and [Fe/H] $= -0.01$. The expected value with adoption of the v_t lowered to 1.30 km s^{-1} (Smiljanic et al. 2009) is +0.03.

If we adopt the parameters tied to either temperature scale of Santos et al. (2009) for analyzing our spectra for the three giants common to the two studies, [Fe/H] estimates for KGP 1175, 1374, and 1461 are increased by $+0.12 \pm 0.02$ dex for the cooler scale and $+0.15 \pm 0.02$ dex for the hotter scale. If the offsets are applicable to the entire giant sample, our metallicity from the giants becomes [Fe/H] $= -0.05$ and -0.02, respectively, the same values found by Santos et al. (2009). Note that the very

good agreement among the abundance estimates when the same stellar parameters are applied weakens the argument that the discrepancy among the studies is a byproduct of underestimated EW from spectra of lower resolution and S/N compared to those available to Santos et al. (2009).

The good news, therefore, is that the high-dispersion spectra for giants discussed to date, when processed using the same fundamental parameters, will generate Fe abundances that are similar at a level typically ±0.02 dex. The bad news is that for a fixed temperature scale, the absolute abundance scale is dominated by the adopted microturbulence velocity, v_t, which leads to a range from [Fe/H] = 0.05 to −0.30 for v_t between 1.3 and 1.9 km s^{-1}.

A potential handle on the location of the zero point of the metallicity scale comes from the observation by PRP of two stars in the Hyades, for which they derive [Fe/H] = +0.06. Since the temperature scale for the Hyades giants as defined by Alonso et al. (1999) is virtually identical to that of Ramírez & Meléndez (2005), the modification applied to the NGC 3680 abundances due to the altered photometry, reddening, and metallicity does not apply. Thus, any remaining offset should be a byproduct of the adopted v_t. Assuming the same formulation applied to derive v_t for NGC 3680 results in the same systematic offset when applied to the Hyades, if one adopts a metallicity for the Hyades near the higher end of the traditional values, [Fe/H] = +0.15, this shifts the PRP corrected abundance for NGC 3680 from −0.29 to −0.20, still out of range of solar abundance but a respectable match to the value derived in this study. We will return to this question again after the discussion of the results for the dwarfs.

3.6. The Dwarfs

For the 13 stars at the turnoff with S/N above 70, the average [Fe/H] = −0.04 ± 0.11, while Si, Ca, and Ni have [A/H] = −0.06 ± 0.10, −0.17 ± 0.12, and −0.12 ± 0.11, respectively. As noted earlier, the scatter among the abundances is predictably correlated with S/N. If the analysis is limited to the five stars in Table 3 with S/N above 110 (boldface ID), the Fe, Si, Ca, and Ni abundances become −0.07 ± 0.02, −0.13 ± 0.05, −0.22 ± 0.07, and −0.18 ± 0.11, respectively. Within the uncertainties, the abundances are consistent with a scaled-solar distribution.

For comparison, Pace et al. (2008) and Santos et al. (2009) have derived abundances for two G-dwarfs in the cluster from the same spectra, finding [Fe/H] = 0.00 and −0.03 for KGP 1752 and −0.07 and −0.04 for KGP 1050, respectively, leading to an average of [Fe/H] = −0.04, consistent with either value for our turnoff dwarfs. However, for consistency, these estimates deserve closer examination. Unlike the giants, the errors in the dwarf abundances are dominated by the temperature scale and are only very weakly dependent upon v_t. Pace et al. (2008) use three reddening-corrected color indices coupling V to 2MASS JHK photometry, then transferred to T_e using the relations of Ramírez & Meléndez (2005) and averaged to define a photometric temperature. This value supplies the starting point for a grid of stellar atmospheres that are interpolated among the variables until the line abundances show minimal trends with EW, excitation potential, or ionization state.

For star KGP 1050, Pace et al. (2008) determined the photometric temperature to be 6053 K, similar to our $B-V$-based estimate of 6098 K, but hotter than the value adopted in PRP by 174 K. However, the spectroscopic temperature used to estimate the abundance was 6210 K, 112 K hotter than the scale used in our abundance derivation for the dwarfs. Use of our photometric scale would lower the abundance of KGP 1050 to [Fe/H] = −0.16; using the photometric scale of Pace et al. (2008) would shift the value to −0.20. By contrast, Santos et al. (2009) adopt 6134 K, 36 K hotter than our photometric value; use of our scale would reduce their abundance to [Fe/H] = −0.07.

Star KGP 1752 follows a similar pattern in that the spectroscopic temperature (6010 K; Pace et al. 2008) is 84 K higher than the $VJHK$ average (5926 K), but in this case the photometric value is only 10 K hotter than the PRP temperature and 6 K cooler than the estimate in Santos et al. (2009). We have no direct means to tie the star reliably into our temperature scale because its composite $B-V$ color has a dispersion above 0.05 mag, one of the largest among the brighter stars in the photometric catalog. If we assume that the VHK value is comparable to our system, the abundance for this star would decline to [Fe/H] = −0.06 for Pace et al. (2008) and remain unchanged for Santos et al. (2009).

However, there is a more important reason why the results for this star remain questionable and why it was not included in our investigation. The star has a high proper-motion membership probability of 58% and its radial velocity is consistent with being a single-star member of the cluster. Despite this, Nordström et al. (1997) flag the star as a questionable member due to its suspicious position in the CMD. The photometric and spectroscopic temperatures for KGP 1050 and 1752 (Pace et al. 2008) imply a temperature difference between these two stars of 127 K and 100 K, respectively, while the spectroscopic scale of Santos et al. (2009) leads to a difference of 202 K. A typical shift of 110 (200) K requires KGP 1752 to be 0.03 (0.05) mag redder than KGP 1050. On the main sequence, being cooler by this amount should place KGP 1752 almost 0.2 (0.3) mag fainter than KGP 1050. Instead, KGP 1752 is 0.3 mag brighter than KGP 1050, placing it 0.5 (0.6) mag above its expected position in the CMD for a star of its color. If the star is not a binary (for which there is no spectroscopic evidence), it is either a non-member or its structure does not resemble that of a typical solar-type star. For either of the above reasons, any spectroscopic abundance tied to this star remains questionable.

What is the correct metallicity for NGC 3680? From the data obtained solely from this study, the eight giants have [Fe/H] = −0.17 ± 0.07 while the best data for the five high S/N dwarfs imply [Fe/H] = −0.07 ± 0.02, with a simple average of −0.12. If one derives a weighted average tied to the inverse of the standard errors of the mean, [Fe/H] = −0.09. When analyzed adopting the same parameters selected in this investigation, the six red giants of PRP and the one giant of Smiljanic et al. (2009) have [Fe/H] = −0.15 ± 0.08 and −0.13 ± 0.10, respectively. As emphasized previously, the problem with the giants is that by an appropriate choice of v_t, the mean metallicity could easily be raised to solar or higher. The one definitive dwarf member analyzed outside this investigation, when placed on our temperature scale, has [Fe/H] between −0.07 (Santos et al. 2009) and −0.16.

From past work, the exclusive metallicity estimate for the dwarfs for over 15 years was the $uvby$Hβ-based value of +0.1 of Nissen (1988), reproduced using the same photometric zero points by Anthony-Twarog et al. (1989) and Bruntt et al. (1999). More recently, the $uvbyCa$Hβ CCD study of ATT identified a possible error in the m_1 photometry of the earlier work and obtained a second metallicity estimate using the independently calibrated hk index. From 34 stars at the turnoff using both photometric indices, m_1 and hk, the cluster metallicity is found

to be [Fe/H] = −0.14 ± 0.03 on a scale where M67 and the Hyades are found to have [Fe/H] = −0.06 and +0.12, respectively (Nissen et al. 1987). For the giants, Twarog et al. (1997) used the combined observations on the DDO system with the moderate-dispersion spectra of Friel & Janes (1993), transformed to a common metallicity scale, to obtain [Fe/H] = −0.10 ± 0.06 from 12 measurements. On the same metallicity scale tied to DDO photometry and moderate-dispersion spectra, 36 measurements for giants in M67 produce [Fe/H] = 0.00 ± 0.09. Twarog et al. (1997) also provide a possible avenue for constraining the zero-point scatter among the various high-dispersion abundances for the cluster dwarfs and giants. Santos et al. (2009) investigate the relative abundances between dwarfs and giants in 13 open clusters, finding a small effect with metallicity that is readily corrected. Of the 13 clusters, 12 are included in the catalog of Twarog et al. (1997). For these 12 clusters, the average difference in [Fe/H], in the sense (santos–taat), is 0.033 ± 0.050 dex. The expected scatter from the quoted errors for the individual abundance estimates is ±0.046 dex. If the residuals are weighted by the inverse errors, the mean offset rises to 0.042 dex. With [Fe/H] = −0.04 from three giants in NGC 3680, the result of Santos et al. (2009) becomes [Fe/H] = −0.08 on the system of Twarog et al. (1997) where, again, the NGC 3680 giants were found to have [Fe/H] = −0.10 ± 0.02 (sem) from 12 spectroscopic and DDO measurements.

An average of the various abundance estimates without regard to zero point and weighted by the inverse of the errors is dominated by the dwarfs: [Fe/H] = −0.08 ± 0.02 (sem). Adoption of values between [Fe/H] = −0.12 and −0.04 have little impact on our conclusions regarding the Li abundances. A change in [Fe/H] of ±0.04 will have a small effect on the ages (∓0.1 Gyr), distance moduli (±0.05 mag), and Li-dip masses (±0.03 $M_{\odot}$).

4. THE Li-DIP: CLUSTER DATA

4.1. NGC 3680

With the establishment of a plausible set of cluster properties for NGC 3680, we can now attempt to place the cluster's Li-dip in the context of the physical parameters that define the dip and its evolution over time. The key papers that have dealt with this issue previously in a comprehensive manner are Balachandran (1995) using open clusters and Chen et al. (2001) evaluating field dwarfs. In a discussion of the pattern of A(Li) in several open clusters, Balachandran (1995) concludes that the masses of the stars in the dip depend on metallicity, but the ZAMS surface temperatures of the stars within the dip do not. The temperature range of the dip appears to depend less on metallicity than on age, based on a comparison of Praesepe and the Hyades, two clusters of similar age but supposedly different metallicity, a point we will return to below. Chen et al. (2001) similarly find that the location of the dip is metallicity dependent and derive a relation for the mass of the central dip stars as a function of [Fe/H], with solar metallicity dip stars having masses near 1.4 $M_{\odot}$, declining to 1.1 $M_{\odot}$ at [Fe/H] = −1.0.

The canonical illustration of the main-sequence Li-dip is a plot of Li abundances versus main-sequence surface temperature or color. For clusters as old as NGC 3680, beyond illustrating the difference in Li between the main sequence and the evolved giants, this representation provides little insight since evolution has shifted the Li-dip into the vertical strip at the CMD turnoff (Daniel et al. 1994; Balachandran 1995). The more functional approach is to use V as the discriminator of mass, keeping in mind the potential confusion caused by binary systems. The relevant diagram using our merged and homogeneous sample for NGC 3680 is shown in Figure 4. Filled circles and triangles represent stars with detectable Li and upper limits, respectively, for stars in our sample, averaged with PRP where available. Open circles and triangles show stars with detectable Li and upper limits, respectively, from the sample of PRP alone. With the sample boosted from 18 to 40 stars, the features defining the Li distribution among the turnoff stars in NGC 3680 are enhanced and expanded. Keeping in mind that binarity can shift the position of a star in the diagram by, at most, 0.75 mag to the left and the predominance of upper limits for Li estimates within the dip region, the location of the center of the dip is reasonably defined as V = 13.45 ± 0.15. This approximate location is obtained by giving significant weight to the distribution of measured Li abundances that comprise the wings of the dip rather than the upper limits that dominate the core of the dip. The midway point between the wings is between V = 13.5 or 13.6. Taking into consideration the fact that the drop in Li is normally somewhat steeper on the high-mass side, this was adjusted to a central dip at 13.45, though clearly values as high as 13.6 are plausible, as defined by the error estimate. A more exact definition of the location of the dip center would require an increase in cluster members (not possible) or the superposition of data from clusters of comparable age and composition, the focus of Section 5.

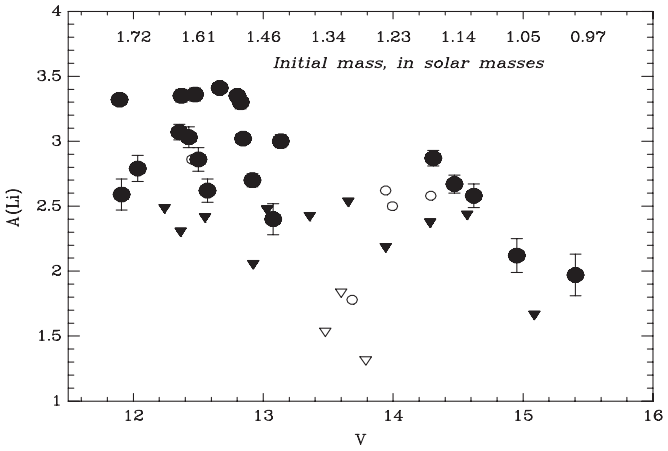

Figure 4. A(Li) vs. V for stars in NGC 3680. Filled circles and triangles are stars observed in this survey with detectable Li and upper limits, respectively, combined with the data of PRP if the samples overlap. Open circles and triangles are stars with detectable Li and upper limits, respectively, observed only by PRP but transferred to our temperature and Li scale.

From the minimum in the Li-dip, the Li abundances for higher mass stars rise steeply to an upper bound of A(Li) = 3.35 by V = 12.85, maintaining this high value to at least V = 12.4. There is one star (KGP 1035) at the Li upper bound at V = 11.9; it is classed by Nordström et al. (1997) as an SB2 and its position in the CMD places it in an evolutionary phase that is so rapid that it is highly likely this star has been shifted to smaller V from a true position between V = 12.4 and 12.8 by its composite nature. By contrast, the one star brighter than the red hook in the turnoff which shows no evidence of binarity (KGP 1522) has A(Li) = 2.80, almost a factor of 4 below the upper bound. This is consistent with a significant Li reduction as stars evolve through the hydrogen-exhaustion-phase toward the red giant branch, where the highest Li abundances are reduced by over two orders of magnitude relative to the upper bound (Pasquini et al. 2004). When contrasting observation and theory

for clusters of this age, it is important to remember that the exact shape of the turnoff hook depends very sensitively on the treatment of convective core overshoot in the models.

On the lower mass side of the dip, the Li abundance rises almost as rapidly, reaching a maximum at $A(\mathrm{Li}) = 2.75 \pm 0.15$ near $V = 14.2 \pm 0.1$, with seemingly little scatter. Toward fainter V, the Li abundance declines by an order of magnitude, reaching a value near $A(\mathrm{Li}) = 1.8$ by $V \sim 15.2$.

For purposes of constraining the dip and its evolution, the V dependence of the 1.8 Gyr isochrone in Figure 3 has been converted to a mass scale, as illustrated along the top of the plot in Figure 4. Based on the V–mass relation, the ZAMS mass of the stars that occupy the center of the Li-dip is $1.35 \pm 0.03\ M_{\odot}$. The current edges of the dip range between $1.51 \pm 0.03\ M_{\odot}$ at the high end and $1.19 \pm 0.02\ M_{\odot}$ at the low end. If we were to transform this mass range to a main sequence at [Fe/H] = −0.08 at the age of the Hyades (0.7 Gyr), the colors coupled to these mass points would be $B - V = 0.40$, 0.32, and 0.50, respectively.

4.2. NGC 752

The first and most straightforward comparison for NGC 3680 is with the very similar open cluster, NGC 752. Building upon the extensive discussion in ATT, the key issue in this, as in any, comparison is *how* similar. There is little disagreement over the relative reddening of the two clusters. Typical estimates for NGC 752 range between $E(B - V) = 0.02$ and 0.04, while NGC 3680 currently is bracketed by 0.05 to 0.07. We will assume $E(B - V)$ for NGC 752 = 0.035, consistent with our earlier work. The more contentious issue is the metallicity. An early evaluation of the state of the metallicity measures for the cluster including standardization and reanalysis of all available photometric data was undertaken by Twarog (1983) and updated and expanded to include spectroscopic data by Daniel et al. (1994), leading to a composite [Fe/H] of −0.15, with significant weight given to the spectroscopic results. Photometric zero-point issues aside, this conclusion would imply an abundance comparable to NGC 3680. Due to improved calibrations, better zero-point photometric checks, and expanded spectroscopic data, the earlier results have gradually been superseded, with a modest change in the answer. Using the combined homogeneous results from DDO photometry and moderate-dispersion spectra of the giants (Twarog et al. 1997) in the manner outlined in Section 3.6 for NGC 3680, the metallicity of NGC 752 is found to be [Fe/H] = −0.09 ± 0.07 from 16 measures. It should be emphasized in this particular case that, unlike NGC 3680, the DDO result (−0.16) differs from that of the spectroscopy (−0.05) by more than 0.1 dex. A significant improvement occurs in the results from $uvbyH\beta$ photometry, where the m_1 data of Twarog (1983) exhibited a systematic offset compared to that of Crawford & Barnes (1970) and Nissen (1988), thereby generating an abundance below [Fe/H] = −0.2. With the resolution of the zero-point question (Joner & Taylor 1995), the mean [Fe/H] of NGC 752 on the $uvbyH\beta$ system is well established at −0.08 ± 0.11 from 31 stars, on a scale where NGC 3680 has [Fe/H] = −0.17 from m_1 data alone and M67 and the Hyades are at −0.06 and +0.12, respectively. Recently, Anthony-Twarog & Twarog (2006) observed NGC 752 for the first time on the extended $uvbyCa$ system and, from 10 single-star members at the cluster turnoff, find $[\mathrm{Fe/H}] = -0.06 \pm 0.09$ on a scale where the Hyades has [Fe/H] = +0.12.

Despite its proximity to the Sun, there have been surprisingly few spectroscopic studies of stars within NGC 752. At high dispersion, Hobbs & Thorburn (1992) find [Fe/H] = −0.09 ± 0.05 from eight turnoff stars on a scale where similar analysis in M67 generates [Fe/H] = −0.04 ± 0.12 for five dwarfs (Hobbs & Thorburn 1991). The high-dispersion data of Sestito et al. (2004) for three stars imply [Fe/H] = +0.01 ± 0.04 from seven dwarfs, on a scale where the Hyades has [Fe/H] = +0.14 ± 0.06, based on three stars. A similar analysis from the same group (Randich et al. 2006) leads to [Fe/H] = +0.03 ± 0.03 from 10 stars in M67 on a scale where one Hyades star gives [Fe/H] = +0.13. While Sestito et al. (2004) dismiss all previous metallicity estimates as either irrelevant or unreliable, a careful analysis confirms that they are remarkably consistent, with most comparisons of the absolute scale distorted by differences among the metallicity zero points. A classic example is presented by the moderate-dispersion work of Friel & Janes (1993) and Friel et al. (2002) where cluster abundances are derived with a zero point for the metallicity scale defined so that M67 has [Fe/H] = −0.09 in the original analysis and is fixed at [Fe/H] = −0.15 in the latter paper. Any comparison of the results from these papers to a spectroscopic scale where M67 is observed to have [Fe/H] = +0.03 will lead automatically to a spurious discrepancy if no zero-point correction is applied.

From the discussion above, the qualitative pattern that emerges is that NGC 752 is more metal-rich than NGC 3680, but more metal-poor than M67. A weighted average of the above techniques leads to [Fe/H] = −0.05 ± 0.04 on a scale where M67 has [Fe/H] = 0.00 and the Hyades is at +0.12.

With the reddening and metallicity differential set, we can now make use of the results of ATT to place the clusters on the same apparent magnitude scale. By direct superposition of the cluster CMD's, ATT found that the apparent modulus of NGC 752 had to be 1.90 mag smaller than that of NGC 3680, assuming they had the same metallicity. With a higher [Fe/H], the main sequence of NGC 752 should be brighter than that of NGC 3680 by approximately 0.03 mag, reducing the offset to 1.87 mag. With the derived $(m - M)$ for NGC 3680 set at 10.30, this implies $(m - M) = 8.43$, a boost from the value of 8.30 found in ATT. Using an appropriately interpolated set of Y^2 isochrones for the slightly higher metallicity adopted for NGC 752, the age of the cluster becomes 1.45 ± 0.1 Gyr, as shown in Figure 5, a slight reduction from the value of 1.55 Gyr derived in ATT. Note that the typical position of the giants is blueward of the first-ascent relation by 0.07 mag.

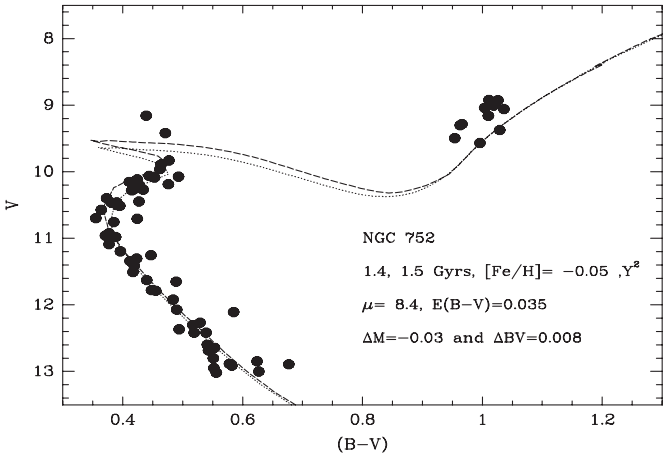

Figure 5. CMD for NGC 752 superposed upon Y^2 isochrones with [Fe/H] = −0.05, $(m - M) = 8.4$, and $E(B - V) = 0.03$, and ages of 1.4 Gyr and 1.5 Gyr. Known binaries and non-members have been removed from the CMD.

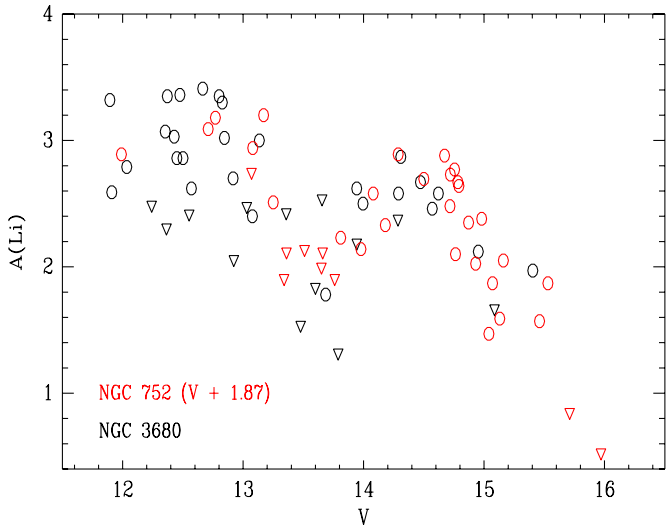

Figure 6. Combined Li data for NGC 3680 (black symbols) and NGC 752 (red symbols). Circles are detected values, while triangles are upper limits.

The combined Li data for NGC 3680 (black symbols) and NGC 752 (red symbols) are shown in Figure 6, with the data for NGC 752 shifted to the distance of NGC 3680. The data for NGC 752 are compiled from Hobbs & Pilachowski (1986), Pilachowski & Hobbs (1988), and Sestito et al. (2004). Because each of these NGC 752 studies listed equivalent widths for the Li line, we were able to analyze the data in a manner consistent with our treatment of our own measures of Li in NGC 3680, including use of the temperature–color calibration described above. A metal abundance [Fe/H] = −0.05 was assumed for this purpose, with a reddening value of $E(B-V) = 0.035$ applied to $(B-V)$ colors compiled by Daniel et al. (1994). For two of the three stars for which equivalent width measurements by Sestito et al. (2004) replicated measures by Hobbs & Pilachowski (1986) and Pilachowski & Hobbs (1988), the resulting Li abundance estimates were averaged. For one of the stars, P859/H207, the published equivalent widths are widely discrepant. The measured equivalent width published by Sestito et al. (2004) was used to compute the Li abundance for this star.

From Figure 6, the morphological agreement between the two clusters is impressive. There is a clear gradient in the upper bound relation as one moves from the brighter stars to the fainter main sequence. The Li abundance pattern near the solar system Li value is, within the errors, the same for both clusters among the higher mass stars above the gap. The sample of stars in NGC 752 with measured Li in this CMD region is frustratingly small; we would predict that a larger sample of observations of stars at the turnoff for V brighter than 11.4 in NGC 752 would produce a pattern identical to that in NGC 3680 unless parameters other than age and metallicity are at work.

Moving down the turnoff, the Li-dip is defined at the high-mass edge by a steep drop at $V = 13.2$, in contrast with the low-mass edge which shows a gradual rise from $V = 13.6$ to $A(\mathrm{Li}) = 2.8$ at $V = 14.25$. Toward lower masses, the small sample in NGC 3680 meshes perfectly with the decline observed in NGC 752. One potential point of concern could be the fact that the Li-dips superpose so smoothly even though NGC 3680 is 0.3 Gyr older than NGC 752 on the current scale. However, the mass of the stars within the Li-dip is low enough that between 1.45 Gyr and 1.75 Gyr the position of the dip shifts to brighter M_V by less than 0.05 mag. Taking into account the slightly higher metallicity of NGC 752 relative to NGC 3680, the mass of the dip stars in NGC 752 should be slightly higher, so the stars should be slightly more evolved at the same age compared to a cluster with lower [Fe/H]. Thus, we expect that the metallicity effect decreases the impact of the age difference to a level which is below detectability for the current sample.

4.3. IC 4651

As noted in the Introduction, any discussion of NGC 3680 or NGC 752 invariably leads back to the third member of the trio, IC 4651. While a common approach is to superpose the Li data of IC 4651 upon that of NGC 3680 and NGC 752, the higher metallicity of this cluster provides an equally important handle on the evolution of the Li-dip and the reliability of predictions based upon the adopted theoretical isochrones. Based on the masses and projected evolution of stars in the Hyades Li-dip and turnoff, are the observations of the Li-dip stars in the ∼1 Gyr older but chemically similar IC 4651 consistent?

The preliminary step is to place IC 4651 on the same parametric scale as NGC 3680 and NGC 752. Unlike NGC 3680, there has been remarkable consistency in the estimation of the cluster parameters from both photometry and spectroscopy. On the photometric side, independent investigations of the cluster on the $uvbyH\beta$ system, Anthony-Twarog & Twarog (1987, 2000) and Nissen (1988); Meibom (2000); Meibom et al. (2002), have exhibited none of the zero-point issues identified for NGC 3680 and have always indicated that the cluster is similar in metallicity to the Hyades. Equally consistent are the reddening estimates tied to the $H\beta$ photometry of Anthony-Twarog & Twarog (1987, 2000) and Nissen (1988). When analyzed using the same intrinsic color relations, the two data sets produce $E(b-y) = 0.071$ and 0.076, respectively, equivalent to $E(B-V) = 0.10$ and 0.11. With these reddening values, Anthony-Twarog & Twarog (2000) and Meibom et al. (2002) find [Fe/H] = +0.12 and +0.13, respectively, the latter after adjusting the m_1 values of Nissen (1988) downward by 0.005 mag to coincide with the their CCD survey. Likewise, DDO data for 11 giants leads to $E(B-V) = 0.11$, and a corresponding [Fe/H] = +0.10 ± 0.05 (Twarog et al. 1997).

On the spectroscopic side, Carretta et al. (2004) analyzed four giants to derive [Fe/H] = +0.11 ± 0.01, assuming $E(B-V) = 0.083$; adoption of a higher reddening raises this estimate. Pasquini et al. (2004) discuss high-dispersion spectroscopic analysis of over 20 stars ranging from giants to G dwarfs and obtain [Fe/H] = +0.10 ± 0.03 with an adopted $E(B-V)$ between 0.12 and 0.13. Finally, from three giants and five dwarfs, Santos et al. (2009) derive [Fe/H] = +0.15 ± 0.01 and +0.15 ± 0.02, respectively.

For the apparent distance modulus, the consistency among recent determinations tied to main-sequence fitting has been equally impressive, with one notable exception which will be discussed below. Twarog et al. (1997) find $(m-M) = 10.25$ for [Fe/H] = +0.1 and $E(B-V) = 0.11$ and ATT derive $(m-M) = 10.20$ with reddening reduced to 0.10. Given the similarity of the cluster metallicity to the Hyades, one can avoid the usual issues with isochrones by doing a direct comparison to the Hyades. Using the Vby data, Anthony-Twarog & Twarog (2000) find $(m-M) = 10.30$ for $E(b-y) = 0.071$ ($E(B-V) = 0.10$) and from the Vvy diagram to much fainter magnitudes, Meibom (2000) finds $(m-M) = 10.36$ for $E(b-y) = 0.076$ ($E(B-V) = 0.11$).

While the cluster parameters are exceptionally consistent internally, one minor discordant note has been raised by recent

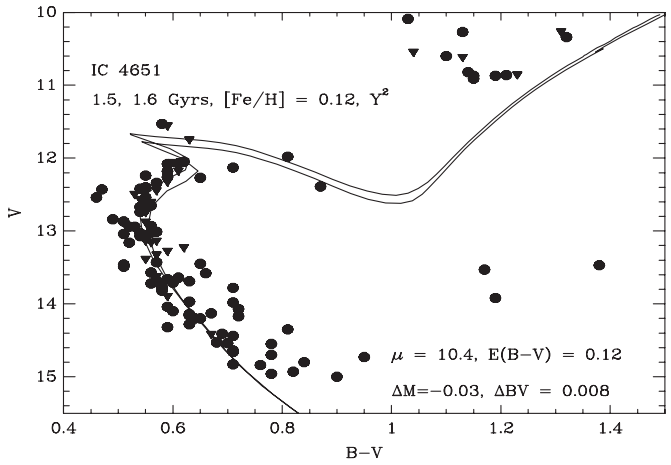

Figure 7. CMD for IC 4651 superposed upon a 1.5 Gyr isochrone with [Fe/H] = +0.15, $(m - M) = 10.4$, and $E(B - V) = 0.12$. Triangles are stars identified as spectroscopic binaries. Known non-members have been removed from the CMD.

high-dispersion spectroscopic work on the cluster. Pasquini et al. (2004), Biazzo et al. (2007), and Pace et al. (2008) have used temperatures based upon consistency constraints on abundances from the multiple lines of differing equivalent width, ionization state, and excitation potential to imply that the reddening value of IC 4651 is closer to $E(B-V) = 0.12$ to 0.13. This conclusion is contradicted by a similar approach applied to the red giants by Carretta et al. (2004) and severely weakened by the analysis of Santos et al. (2009), who generate the same abundances but two distinctly different temperature scales for the same stars using two different line lists. Ultimately, the differences between the higher reddening value and $E(B - V) = 0.10$ discussed in Anthony-Twarog & Twarog (2000, 2004); Meibom et al. (2002) and $E(B - V) = 0.11$ discussed in Meibom (2000) and Twarog et al. (1997) are minor and well within the error bars of both approaches. If we adopt $E(B-V) = 0.12$ for IC 4651, $E(b-y)$ becomes 0.085; shifting from the older average of $E(b - y) = 0.073$ leads to a correction to m_1 of an additional 0.004 mag, raising [Fe/H] for IC 4651 on the Strömgren system to [Fe/H] = +0.16, again, not a statistically significant change from earlier results. With a reddening of $E(B - V) = 0.12$, the apparent modulus rises to $(m - M) = 10.40 \pm 0.05$. Under the assumption that IC 4651 has a metallicity indistinguishable from that of the Hyades and using an appropriately interpolated set of Y^2 isochrones ([Fe/H] = 0.15), $E(B - V) = 0.12$ and $(m - M) = 10.40$, as illustrated in Figure 7, the age of the cluster becomes 1.50 ± 0.1 Gyr, a reduction from the value of 1.75 Gyr derived in ATT and 1.7 Gyr in Meibom et al. (2002) due to the higher adopted reddening, a slightly higher absolute [Fe/H], and exact interpolation of the isochrones. Triangles are stars known to be spectroscopic binaries; known non-members have been removed from the sample which is a combination of the BV photographic and CCD data in Anthony-Twarog et al. (1988). It should be noted that the color and magnitude offsets applied to the isochrones for NGC 3680 have also been applied to the sets at higher [Fe/H]. A consistency check has been made by matching the photometry of the Hyades (Joner et al. 2006) to an isochrone of appropriate age and $(m - M) = 3.33$, with the offsets included; the agreement is excellent.

The comparison between the data and the isochrones is encouraging, especially at the red hook in the turnoff which is dominated by the assumed degree of convective overshoot mixing. Note, however, that the giants all lie blueward of the first-ascent giant branch, in sharp contrast with NGC 3680 and as predicted if the giants are dominated by He-core-burning stars. This difference with NGC 3680 could be removed by altering the reddening of IC 4651 to a value closer to $E(B - V) = 0.00$, thereby requiring a reduction in the apparent modulus by 0.6 mag and significantly boosting the cluster age. As discussed previously, however, reductions in the reddening go opposite to the trend from spectroscopy in recent years.

Before the IC 4651 data are linked to younger clusters of the same metallicity, the particularly anomalous results of Biazzo et al. (2007) need to be addressed. The focus of their study is the use of line-depth-ratios from high-dispersion spectra of giants to derive temperatures which, when combined with absolute magnitude and metallicity, can generate a mass and, ultimately, through isochrone comparisons, an age. The problem is that Biazzo et al. (2007) quote an age of 1.4 Gyr and an apparent modulus of $(m - M)$ of 9.83 for IC 4651 from a comparison to the Padova isochrones. We have reproduced the comparison of Figure 7 using properly interpolated and zeroed Padova isochrones and find excellent agreement with the age and modulus obtained from the Y^2 isochrones, as expected from the comparison with ATT. The Biazzo et al. (2007) age estimate should be adjusted downward to correct for their use of [Fe/H] = 0.10, if their results are to be compared with our adopted [Fe/H] = 0.15. Clearly, however, an estimate of $(m - M) = 9.8$ is implausible given the discussion above and the fit in Figure 7; the minimum modulus using the lower limit to the reddening, $E(B - V) = 0.085$, is 10.15, as derived in Anthony-Twarog & Twarog (2000) and adopted by Carretta et al. (2004), and can only increase for higher reddening. Biazzo et al. (2007) make no note of this apparent anomaly, citing only two dated references (Nissen 1988; Kjeldsen & Frandsen 1991) that are consistent with their result. The primary source of the problem comes from their use of the photometry of Piatti et al. (1998) to compare the cluster CMD to the theoretical isochrones. As discussed in Anthony-Twarog & Twarog (2000), the V magnitudes in this survey are systematically too bright by 0.20 mag. Even worse, the V zero points between the two CCD fields studied in the cluster differ by 0.09 mag. Because no additional $V-I$ colors are available for comparison, any attempt to use their $V-I$ CMD to derive an age by matching to isochrones must be highly questionable, making the approximate agreement between 1.4 Gyr and Figure 7 purely fortuitous.

4.4. Hyades and Praesepe

As a younger Li standard for comparison purposes, we have combined data for the Hyades and Praesepe. There is no question that the Hyades is metal-rich, with [Fe/H] values noted in this paper between +0.12 and +0.17; we have selected +0.15 for the temperature scale. What matters, however, is that IC 4651 and the Hyades be the same within ±0.05 dex. The more controversial cluster is Praesepe. Following the same sources discussed for the other clusters, DDO photometry of four giants produces [Fe/H] = $+0.14 \pm 0.07$ and $E(B - V) = 0.0$ (Twarog et al. 1997). $uvbyH\beta$ photometry of Nissen (1988) implies $E(B - V)$ less than 0.01 and [Fe/H] = $+0.10 \pm 0.15$ from 42 dwarfs on a scale where the Hyades has [Fe/H] = +0.12, consistent with the earlier results of Crawford & Barnes (1969). Joner & Taylor (1995, 2007) derive an offset of ∼+0.01 mag to the m_1 index of Crawford & Barnes (1969), which would imply a higher [Fe/H]. Washington photometry of four giants in each

of the Hyades and Praesepe clusters leads to +0.07 and +0.04, respectively (Geisler et al. 1991).

Spectroscopically, the high-dispersion standard for some time has been tied to three related papers (Boesgaard & Budge 1988; Boesgaard 1989; Friel & Boesgaard 1992). The first investigation found [Fe/H] = +0.13 ± 0.07 (sem) from five single dwarfs, on a scale where F dwarfs in the Hyades had [Fe/H] = +0.17 ± 0.06 (sem). The latter two studies generate a combined [Fe/H] = +0.06 ± 0.06 from seven dwarfs on a scale where the Hyades has [Fe/H] = +0.13; a weighted average combining these two samples raises the Praesepe value to +0.09 ± 0.03 (sem) (An et al. 2007). More recently, An et al. (2007) used four dwarfs to derive +0.11 ± 0.06, on a scale where the Hyades has [Fe/H] = +0.13, while Pace et al. (2008) obtain +0.27 ± 0.10 from seven dwarfs. As a final note to the summary from the literature, Taylor (2006) has attempted a rigorous assessment of the reddening of the Hyades, Coma, and Praesepe and concludes that while the former two clusters have effectively no reddening, Praesepe has $E(B-V) = 0.027$. His reevaluation of past high-dispersion work in this context implies [Fe/H] = +0.01 ± 0.04 for the cluster.

With the exceptions of Taylor (2006) and Pace et al. (2008) at opposite ends of the metallicity limits, there is general agreement that Praesepe is metal-rich compared to the Sun and similar to, or slightly lower than, the Hyades. This meshes well with the high-dispersion analysis of a few dozen Praesepe dwarfs by the Indiana group which, when processed on the same temperature scale as NGC 3680 with $E(B-V) = 0.0$, leads to [Fe/H] = +0.144 on a scale where the Hyades has [Fe/H] = +0.15.

The results for the combined Li data for the Hyades and Praesepe (Steinhauer 2003) are shown as a function of $B-V$ in Figure 8. Blue circles and red squares are the Hyades and Praesepe data with measured abundances, respectively, while the blue and red triangles are upper limits. The original EW data for Li in the Hyades are from Thorburn et al. (1993), Boesgaard et al. (1988), Boesgaard & Tripicco (1986a), and Soderblom et al. (1990), while the Praesepe data are from Boesgaard & Budge (1988), Soderblom et al. (1993), and Burkhart & Coupry (1998). The EW data have been converted to A(Li) using the same approach adopted for NGC 3680. The $B-V$ colors for Praesepe are from Johnson (1952) and Mendoza (1967); both sets of photometry are in excellent agreement with each other. For the Hyades, we have adopted the photometry of Joner et al. (2006) whenever possible. Joner et al. (2006) identify the need for a zero-point shift of +0.008 mag for the more commonly used data from Johnson & Knuckles (1955); for stars for which only the photometry of Johnson & Knuckles (1955) is available, this offset has been applied.

Though it is by no means perfect, the agreement between the superposed data is impressive, especially in the region of the Li-dip. The one obvious disagreement is in the $B-V$ region between 0.55 and 0.6. Praesepe exhibits a population of stars that has clearly depleted the surface Li by a significant amount compared to the well-defined upper bound in this color range. The depletion is non-uniform among the Praesepe stars, with one star reaching a factor of 20 below the expected value, and it is not present in the less populous sample from the Hyades. In the region of the Li-dip, however, we have drawn by eye a mean relation through the combined sample, as illustrated by the solid line. Within the center of the Li-dip, the points defining measured Li abundances have been given significantly more weight than the points with only upper limits. Three conclusions

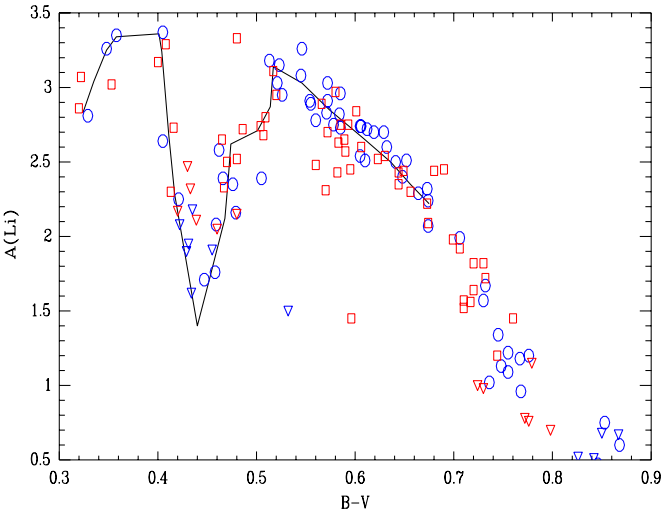

Figure 8. A(Li) as a function of $B-V$ for stars in the Hyades (blue symbols) and Praesepe (red symbols). Circles are detectable values of Li, while the triangles are upper limits. Solid line is an estimate of the mean relation through the points in the region of the Li-dip.

emerge from the mean relation: (a) the $B-V$ center of the Li-dip is the same for both clusters at 0.44 ± 0.01. For this metallicity and age, the isochrones predict that the stars at this point will have a mass of 1.421 ± 0.015 $M_{\odot}$; (b) the high mass limit of the dip occurs precipitously at $B-V = 0.405 \pm 0.005$, equivalent to 1.494 ± 0.008 $M_{\odot}$, while the low-mass boundary occurs at $B-V = 0.517$ and a mass of 1.28 $M_{\odot}$; and (c) the Li-dip is not symmetric. In particular, there is evidence that in the color range from $B-V = 0.47$ to 0.52, Li depletion has occurred at a higher rate than for stars just redward of this region, creating a secondary dip among these stars on the main sequence.

If we assume that the Li-dip profile as defined by the Hyades and Praesepe represents that of IC 4651 at the same age, we can now translate this relation to the age, distance, and reddening of IC 4651 and see how they compare. The initial step is the evolution of the Li-dip to the age of the cluster. This is done by converting the Li–$(B-V)$ relation to an Li–mass relation, then converting it to an Li–M_V relation at the age of IC 4651. With the apparent modulus known, this readily translates into a predicted location for the Li-dip in the CMD turnoff region. The expectation is that the center of the dip should occur at the appropriate magnitude but, at best, the IC 4651 data should lie at or below the mean relation at a given V due to potential depletion in Li between an age of 0.7 Gyr and 1.5 Gyr. The Li data for IC 4651 come from three sources, Pasquini et al. (2004), Balachandran et al. (1991), and unpublished data from S. Balachandran (1990, private communication). Of these several sources, only Pasquini et al. (2004) list measured equivalent widths as well as final abundances and stellar temperatures. We employed $(B-V)$ colors from Anthony-Twarog et al. (1988) to compute temperatures for the dwarf stars consistent with our analysis path for NGC 3680 and NGC 752, using a reddening value $E(B-V) = 0.12$ and an assumed metallicity of [Fe/H] = 0.15. As Pasquini et al. (2004) list lithium abundances derived for two separate temperatures, one based on photometric colors, the other based on spectroscopic reductions, we were able to adjust the published Li abundances to conform with our temperature scale by applying a correction $\Delta A(\mathrm{Li}) = 7.1 \times 10^{-4} \Delta T$. Results for stars common to more than one source were averaged if both results were derived abundances;

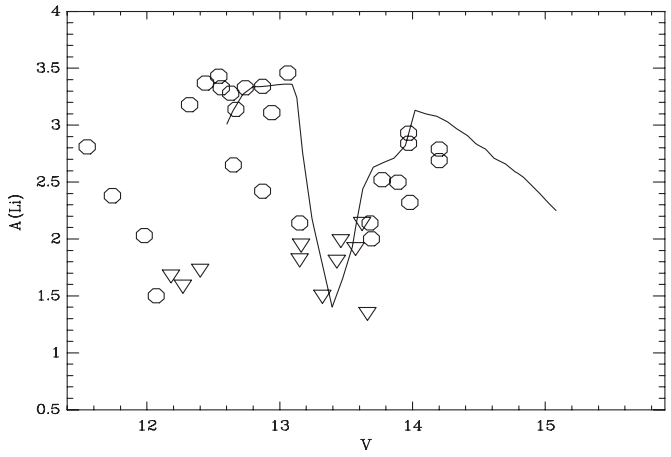

Figure 9. A(Li) as a function of V for stars in IC 4651. Circles are detectable measures, while triangles are upper limits. The solid line is the mean relation of Figure 8 evolved to the age of IC 4651 and shifted in V by 10.25 mag.

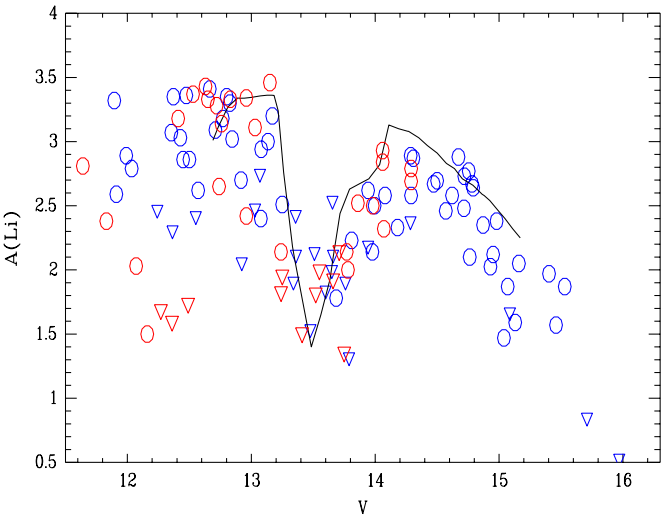

Figure 10. A(Li) as a function of V for the combined cluster sample of Figures 6 and 9. Blue circles are detectable measures, while triangles are upper limits for NGC 3680 and NGC 752; the red symbols have the same meaning for IC 4651. The solid line is the mean relation of Figure 9. The solid relation and the data for IC 4651 have been shifted to fainter magnitudes by 0.09 mag in V.

if either or both results were upper limits, the more stringent upper limit was adopted.

Initial attempts to superpose the predicted Li-dip distribution upon the observed trend in IC 4651 made use of the Padova isochrones and failed in that the predicted location of the Li-dip at 1.5 Gyr was 0.4 mag fainter than observed, implying that the mass center of the Li-dip for the Hyades and for IC 4651 were different. Part of the issue may be tied to the need to adjust the Padova isochrones to our adopted solar color and luminosity, shifting the color for a star on the main sequence at a given mass. While the combined shift was tested for the Hyades and confirmed in that it gave the appropriate distance modulus, it may well be that the relative required combined shifts in $B-V$ and V are different at higher [Fe/H] from what they are at solar metallicity, thereby altering the mass–color relation. The switch to the Y^2 isochrones was made, in part, because the offsets applied to the isochrones are smaller and conceivably would be less affected by alterations at metallicities different from solar. This has proven to be the case. Figure 9 shows the Li distribution for the stars in IC 4651 (open circles are detections while triangles are upper limits) with the Hyades/Praesepe Li-dip relation evolved to an age of 1.5 Gyr and shifted by 10.25 mag, identifying the center of the Li-dip as $V \sim 13.35$. The mass of the stars at this location is 1.47 $M_{\odot}$, larger than the Hyades-based 1.42 $M_{\odot}$ and a predicted Li-dip location of $V = 13.52$. Note that a star with 1.47 $M_{\odot}$ would have $B-V = 0.416$ at the metallicity and age of the Hyades, only slightly bluer than our adopted Li-dip center of $B-V = 0.44$.

Given the small number of stars used to define the IC 4651 profile, the consistency between the shift predicted by the isochrones and the observations is encouraging. On the brighter, high-mass side of the dip, there appears to be no decline from A(Li) values near the solar system value until one reaches the stars evolving through the hydrogen-exhaustion phase and toward the red giant stage. Within the broad uncertainties, the sharp drop seen on the high-mass side remains unchanged. On the low-mass, fainter side, all the cluster stars fall on or below the Li-dip, as expected if some depletion has occurred from the upper limits for these stars as defined by the Hyades relation. Note also that the secondary dip identified within the Hyades will be difficult to verify due to the small sample populating the correct magnitude range.

5. LITHIUM IN OPEN CLUSTERS

5.1. Li-Dip: Structure and Evolution

To optimize the insight gained from the clusters, we combine Figures 7 and 9 in Figure 10. Because the metallicities of NGC 3680 and NGC 752 are so similar and the age difference partially compensates for any evolutionary effect, no adjustment is made to the relative positions of the points (blue) in Figure 7. The combined samples for these two clusters are at an effective true modulus of $(m-M)_o = 10.12$; if the metallicity is lowered to [Fe/H] $= -0.12$, the true modulus is reduced to 10.07. For IC 4651, the true modulus is $(m-M)_o = 10.03$, identical within the uncertainties to the distance to NGC 3680. For consistency, however, we have added 0.09 mag to the V magnitudes for the data points in IC 4651 (red) and the mean relation (solid line) of Figure 9 to place them at the same distance as the other clusters in Figure 10.

Clearly, the Li-dip profile as defined by the combined Hyades and Praesepe data and evolved to an age of ∼1.5 Gyr does an excellent job of mapping out the region of the observed composite Li-dip. Several key features are enhanced in the composite sample. (1) The upper bound at A(Li) = 3.35 for the stars above the Li-dip is well established. One star at the bright edge of the Li-dip sits above the upper bound by only 0.1 dex, an insignificant offset given the errors; (2) keeping in mind that non-interacting binaries will be shifted horizontally to the left and that the sample of stars above the Li-dip is incomplete, the upper bound appears to end abruptly at $V = 12.35$. Stars brighter than this level are leaving the turnoff for the giant branch, either in or beyond the hydrogen-exhaustion phase. It should be emphasized, however, that not every star within the main sequence red hook exhibits reduced Li; (3) the vertical drop in A(Li) on the high mass side of the dip occurs over a very small range in V, consistent with the sharp Hyades/Praesepe drop with color. Likewise, the profile on the low-mass side matches the observational upper bound extremely well. This appears to indicate that over the ∼1 Gyr of evolution between the Hyades and the average age of these clusters, little significant alteration has occurred in the Li distribution within the Li-dip,

implying that the physical process producing the dip may have run its course by 0.7 Gyr. It should be remembered, however, that due to the steepness of the profile and the logarithmic basis of the plot, a drop in Li by a factor of 2 or less would be difficult to detect; (4) with the exception of a handful of stars near $V = 14.7$ in NGC 752, the average star fainter than the Li-dip is typically 0.25 dex lower in A(Li) than the mean relation for the Hyades, though this differential would be cut in half if the mean dip relation were shifted to brighter V magnitudes by 0.15 mag. Within the errors, there does appear to be a modest decline in A(Li) for the cooler dwarfs outside the dip between the ages of the 0.7 and 1.5 Gyr.

To close our discussion of the Li-dip, we can estimate the mass dependence of the center of the dip on metallicity. Our comparison of the Hyades/Praesepe dip ($M = 1.42\,M_{\odot}$) with the evolved location in IC 4651 ($M = 1.47\,M_{\odot}$) implies that, due to the uncertainties in the evolutionary models, independent of the uncertainty in the exact placement of the center of the dip for the older clusters, it is possible that the isochrones will predict too high a mass when matched to the CMD position of the clusters near 1.5 Gyr. For NGC 3680 and NGC 752 at an approximate [Fe/H] $= -0.07$, the mass of the Li-dip center is 1.35 $M_{\odot}$. Contrasting this with IC 4651, a linear relation over this metallicity range would be $M_{\rm dip}/M_{\odot} = 1.38(\pm0.04) + 0.4(\pm0.2)$[Fe/H]. For comparison, using field stars over a much wider range in [Fe/H] and a different set of stellar models, Chen et al. (2001) found $M_{\rm dip}/M_{\odot} = 1.42 + 0.28$[Fe/H].

What is the physical origin of the Li dip and the regions surrounding it? Once the Hyades and field dwarf Li data of Boesgaard & Tripicco (1986a, 1986b) firmly established that F stars depleted far more Li than predicted by standard theory (see discussion in Deliyannis 2000), a variety of mechanisms beyond the SSET were proposed. These loosely fall into three categories: mass loss, diffusion, and slow mixing due to rotation or waves. In the mass-loss scenario, the small outer mass fraction where Li is preserved is simply lost (Schramm et al. 1990). In the original diffusion scenario for the Hyades (Michaud 1986), diffusion is unimportant for surface Li depletion in G dwarfs, but as one goes to the hotter early F dwarfs, the increasingly shallow SCZ allows increasingly efficient draining of the Li out of the base of the SCZ via gravitational settling and thermal diffusion. This creates the red side of the gap. In the middle of the Li gap, Li retains an electron and with its now much larger cross section, Li becomes radiatively accelerated upward, creating the hot side of the gap. However, this can cause large Li overabundances in stars hotter than $B - V = 0.40$ (a "Li peak"), which was not observed, so a finely tuned mass-loss rate was included in such stars to balance the diffusion.[5] The more refined diffusion models of Richer & Michaud (1993) predicted a much narrower Li dip ($\sim$100 K in T_e), which could no longer explain the full width of the observed Li dip ($\sim$300 K for the primary dip and 500 K or more when including the secondary dip), and even less so the more widespread Li depletion hotter and cooler than the dip.

Mechanisms that can drive slow mixing include, (a) waves caused by the SCZ (Garcia Lopez & Spruit 1991; Talon & Charbonnel 2003), and (b) rotation-related effects such as meridional circulation or the onset of angular momentum transport induced primarily by secular shear (Pinsonneault et al. 1990; Chaboyer et al. 1995; Deliyannis & Pinsonneault 1997, collectively referred to as the Yale models). Charbonneau & Michaud (1988) proposed that meridional circulation combined with diffusion could explain the Li dip, though later work suggested that the efficiency of meridional circulation must be greatly suppressed (Charbonneau et al. 1989; Pinsonneault et al. 1990). Another candidate process, turbulent transport, overdepletes stars beyond the hot side of the Li dip when diffusion is allowed for (Charbonneau & Michaud 1990). In the Yale models, surface angular momentum loss acting primarily during the early main sequence of G dwarfs exacerbates differential rotation with depth, which sets off a secular shear instability, causing mixing. Different initial rotation rates cause the observed dispersions in Li abundances. Increasing initial angular momentum with mass and corresponding greater mixing results in the cool side of the dip. But stars progressively hotter than the break in the Kraft curve (which coincides with the middle of the Li dip) lose progressively less angular momentum, thus producing the hot side of the Li dip.

These various classes of models meet with varying degrees of success in reproducing the Hyades Li dip, and distinguishing between them using the Hyades dip alone can be challenging. Fortunately, there exist additional powerful discriminators, that include (a) the timing of the formation of the Li dip and the evolution of its Li-mass morphology, (b) the Li–Be and Be–B depletion correlations, (c) short-period tidally locked binaries, and d) subgiants evolving out of the Li dip, whose deepening convection zones reveal the shape and depth of the Li preservation region of their main-sequence progenitors.

The early onset of Li depletion by factors of 4–6 and over a wide T_e range (6000–6700 K, at minimum) observed in the 150-Myr-old cluster M35 (Steinhauer & Deliyannis 2004) favors the Yale rotational models as the dominant effect at early ages and argues against mass loss or diffusion which require longer time scales. The striking Li-Be depletion correlation discovered in field dwarfs on the cool side of the Li dip (Deliyannis et al. 1998; Boesgaard et al. 2001) and in open clusters (Boesgaard et al. 2004) argues strongly in favor of slow mixing induced by rotation, as in the Yale and other models that produce the specifically observed Li/Be ratio (e.g., Charbonnel et al. 1994), and argues strongly against diffusion (where Li and Be are depleted from the surface at a similar rate) and mass loss (where all the Li must disappear before Be depletion can be observed). The Li–Be correlation can even discriminate among models with slow mixing; for example, the wave-driven mixing in the Garcia Lopez & Spruit (1991) models does not penetrate very deeply, and as a result the predicted Li/Be ratio is too large. The wave-driven mixing of Talon & Charbonnel (2003) is more promising, especially in its association of angular momentum transport by waves, and in its potential to explain the spread of Li abundances as a function of T_e for stars cooler than the Li dip, but it remains to be seen whether more quantitative models can reproduce constraints other than those from Li in the Hyades alone (such as, but not limited to, the constraints described here). Since Be is preserved to roughly twice the depth as Li with B preserved to a depth twice as large again, the observed Be–B depletion correlation further illustrates the depth to which mixing occurs, and further defines its relative efficiency with depth (Chaboyer et al. 1995). Combining the Yale rotational models with Zahn & Bouchet's (1989) tidal circularization theory results in the prediction that tidally locked

[5] Li peak stars may exist after all: Deliyannis et al. (2002) discovered a star in the Hyades-aged cluster NGC 6633 near 7100 K with A(Li) = 4.3, at least an order of magnitude above the assumed initial abundance of the cluster. This is consistent with the diffusion predictions of Richer & Michaud (1993), although other explanations are also possible (Laws & Gonzalez 2003; Ashwell et al. 2005).

binaries with sufficiently short period should exhibit higher Li abundances than single stars because they exchanged angular momentum during the early pre-main sequence when their interiors were not yet hot enough to destroy Li. Thus, they do not exhibit the subsequent mixing and Li depletion induced by angular momentum loss that normal, single stars do. (See also Soderblom et al. 1990.) This prediction is supported by the observation of high-Li short-period binaries above the late-F/early-G Li plateau and elsewhere in the Hyades (Thorburn et al. 1993), in M67 (Deliyannis et al. 1994), and in a variety of other contexts (Ryan & Deliyannis 1995). Li in subgiants in the solar-aged M67 cluster reveal that the Li preservation region during those stars' MS evolution was smaller than that predicted by standard or diffusion models, consistent with that predicted by the Yale rotational models, and larger than that predicted by mass loss. These considerably varied diagnostics all consistently favor slow mixing (probably induced by rotation) as the primary cause of Li depletion in F dwarfs, and consistently argue against mass loss or diffusion.

The present study adds additional interesting constraints that successful mechanisms must meet. The possible delineation of the Li dip into a deep primary and shallower secondary Li dip in the Hyades+Praesepe data, which is also consistent with the Li data in the older clusters NGC3680, NGC 752, and IC4651, suggests that Li depletion occurs fairly early (before 200 Myr), over a wide range of T_e (at least 6000–6700 K) and is caused primarily by rotationally induced mixing, but a more severe Li depletion continues to develop in a more restricted T_e range near 6700 K later but by the age of the Hyades. This further depletion could be caused by or be aided by diffusion. Although two stars with very low Li in the primary Hyades Li dip are also known to have a significant Be depletion (Boesgaard & King 2002), consistent with rotational mixing, the Li data are only upper limits, and thus the Li/Be is not known in these stars, and could allow for the possibility of late Li diffusion, especially at a T_e where the picture gets further complicated by the possibility of upward radiative acceleration of Be (Richer & Michaud 1993), even as Li continues to diffuse downward. Additional Li data, preferably detections, in the deep parts of the primary Li dip, ideally along with Be data, could help cast light on whether diffusion ever contributes to the formation of the Li dip. In NGC 3680 stars hotter than the Li dip, we stress that we have found a Li spread of at least 1 dex in magnitude. That is, these stars do *not* exhibit a constant, presumed undisturbed initial cluster Li abundance. (However, a larger fraction of IC 4651 stars, indeed most of them, are found near the Li upper bound; only three stars have been observed in NGC 752, but they also lie close to the upper bound.) Such a spread in NGC 3680 is not altogether surprising, as the SCZs are *extremely* shallow in these stars, and many complex competing factors can affect the surface Li abundances, including rotationally induced mixing of varying types, diffusion, magnetic fields, and even just tiny rates of mass loss.

5.2. Li in the Giants

While the focus of our study has been the turnoff dwarfs, the added data on the giants in NGC 3680, as well as additional data in IC 4651 (Pasquini et al. 2004), promise potential insight into post-main-sequence evolution of Li as discussed by ATT and Pasquini et al. (2004). For NGC 3680, the sample of PRP has been increased from six to nine giants; all three members of the expanded sample are probable binaries. As emphasized in ATT, the surprising result from the earlier work of PRP was the discovery that while the Li abundances among the giants of NGC 3680 were reduced relative to the turnoff stars, of the six giants studied, four had measurable abundances rather than upper limits, and three of the four measurable values sat near $A(\mathrm{Li}) = 1.0$. This led to a bimodal distribution in A(Li). The combined sample confirms and expands the result. Of the three new giants, two have $A(\mathrm{Li}) = 0.98$ and 1.09, while the third has 0.50. For the nine giants, five have an average A(Li) of 1.08 ± 0.08, while the remaining four have $A(\mathrm{Li}) = 0.45 \pm 0.07$ or an upper limit measurement. It should be noted that the true limit for KGP 1379 is undoubtedly lower since the unusual blue color of this star implies a likely main-sequence turnoff companion. While the Li line strength would be weakly impacted by the companion, the effect of the bluer color is to raise the effective temperature, producing a significant overestimate for Li.

How does NGC 3680 compare to NGC 752? First, of the three clusters, NGC 3680 is clearly the oldest, while NGC 752 and IC 4651 are virtually identical in age if one accepts the higher reddening value for the latter cluster. As discussed in ATT, NGC 752 and NGC 3680 have distinctly different A(Li) distributions among the giants. For NGC 752, of 11 highly probable members on the giant branch, only two have detectable Li abundances, both above $A(\mathrm{Li}) = 1$. The remaining nine stars have only upper limits of 0.5 or less.

Beyond the age difference, the second way in which NGC 752 and NGC 3680 distinctly differ is in the CMD distribution of the giants. A comparison of Figure 3 with Figure 5 shows that the giants in NGC 3680 sit squarely on the first-ascent giant branch in the luminosity range associated with the red giant bump. By contrast, while the giants in NGC 752 occupy a comparable range in luminosity, they sit systematically blueward of the first-ascent giant branch and 0.07 mag bluer in $B - V$ than the typical star in NGC 3680, occupying the CMD area commonly associated with the red giant clump and He-core-burning stars. Finally, the two stars in NGC 752 with measurable Li do not sit among the stars populating the clump, but lie along the red edge of the CMD distribution (see Figure 8 of ATT). A qualitative explanation comes from the observation that some stars evolving through the red hook at the turnoff exhibit reduced Li from the limiting value of 3.35. Note that of all the stars with measured Li in the three clusters, only one star in IC 4651 is situated in the subgiant region of the CMD between the turnoff and the vertical first-ascent giant branch. It has $A(\mathrm{Li}) = 1.5$. All other single stars with reduced Li populate the red hook. The implication is that some form of unexpected mixing, possibly due to enhanced rotation (Pasquini et al. 2004), is destroying the atmospheric Li as the star evolves away from the main sequence and up the giant branch. Thus, first-ascent red giants may still retain a detectable level of Li near $A(\mathrm{Li}) = 1$ as they pass through the red giant bump phase and/or bring new Li to the surface as a byproduct of the interior evolution and mixing that creates the red giant bump. Evolution to the He-core-burning phase reduces A(Li) to 0.5 or lower, unless an alternative source of Li production is found. When coupled with the timescales in the different evolutionary phases, giant branch abundances should show a natural dichotomy. One group of predominantly first-ascent giants will have measurable Li near $A(\mathrm{Li}) = 1$, while the more evolved stars will have $A(\mathrm{Li}) = 0.5$ or less. NGC 752 is dominated by the latter group, NGC 3680 by the former.

Given the pattern above, it is straightforward to predict where IC 4651 should fall in the Li-dichotomy. Its age is effectively identical to NGC 752 but the mass of a typical star on the giant

branch (1.93 $M_{\odot}$) is higher than that for NGC 752 (1.86 $M_{\odot}$) or NGC 3680 (1.75 $M_{\odot}$). The stars on the giant branch, especially with the increased cluster reddening, sit squarely blueward of the first-ascent giant branch by more than 0.1 mag in $B-V$ (Figure 7). The Li distribution among the giants should resemble that of NGC 752. As discussed in ATT using the unpublished data supplied by Suchitra Balachandran, of 11 member giants observed in IC 4651, only one had detectable Li with $A(\mathrm{Li}) = 1$. The other 10 stars only had upper limits, with the limits ranging from $A(\mathrm{Li}) = 1.05$ to -0.1. Pasquini et al. (2004) observed five giants, three of which overlapped with the earlier sample. For the two new giants, the stars had upper limits to A(Li) near 0.2. For the stars in common to the surveys, the newer data showed an upper limit of 0.38 where the older sample found an upper limit of 0.2, a measured value of 0.5 where the older data implied an upper limit of 1.0, and a measured value of 0.82 where the previous result was an upper limit of 0.75. Therefore, of 13 observed stars, one giant definitely has A(Li) at 1.0 with possibly a second near 0.8. Eight more giants have a measured value of 0.5 or an upper limit of 0.7 or less. The remaining three giants have upper limits, but they range between 0.95 and 1.05, so the possibility of detectable Li cannot be ruled out. If we class these last three as unknowns, the fraction of giants with high Li (A(Li) $\sim$1) in IC 4651 is 2 out of 10, statistically the same as in NGC 752.

6. SUMMARY

The specific focus of this study has been the Li abundance distribution of stars at the turnoff of the intermediate-age open cluster, NGC 3680, with the general goals of linking future Li analyses of turnoff stars in NGC 6253 to the larger array of published data in other open clusters while reevaluating NGC 3680 itself in the context of the evolution of the Li-dip. After taking into account the modest differences in the reddening and temperature scales, there is very good agreement with past Li abundance determinations. The combined data set more than doubles the turnoff sample and increases the red giant sample from six to nine stars. The expanded sample better delineates the Li-dip region and reinforces the observed dominance of the giant branch by stars with A(Li) near 1.

Spectroscopic analysis of the red giants in NGC 3680 produces [Fe/H] $= -0.17 \pm 0.07$ from eight stars. Previous giant star spectroscopy gives the same result if the spectra are analyzed with the same stellar parameters. The absolute scale can, however, be set at any value between [Fe/H] = 0.00 and -0.30 by adopting microturbulence velocities between 1.3 km s^{-1} and 1.9 km s^{-1}. For the dwarfs, the scatter is a strong function of the S/N; from five single stars at the turnoff with S/N above 110, [Fe/H] $= -0.07 \pm 0.02$. There is no statistically significant evidence from lines other than Fe that NGC 3680 has anything but scaled-solar elemental abundances. An average of all abundance determinations weighted by the inverse of the standard errors of the mean heavily favors the dwarfs and produces [Fe/H] $= -0.08 \pm 0.02$ (sem). With the reddening and metallicity known, isochrone comparisons require an age of 1.75 Gyr and an apparent modulus of $(m - M) = 10.3$. These data place the center of the Li-dip at a 1.35 $M_{\odot}$.

With the fundamental cluster information in hand, NGC 3680 is contrasted with two slightly younger clusters, NGC 752 and IC 4651, and the even younger clusters, Hyades and Praesepe. Assuming a slightly higher reddening value of $E(B-V) = 0.12$ for IC 4651, with [Fe/H] $= -0.06$ and +0.15 for NGC 752 and IC 4651, respectively, both clusters have an age near 1.5 Gyr, with apparent moduli of 8.43 and 10.4, respectively. For the Li-dip comparisons, the Hyades and Praesepe are both assumed to have zero reddening and [Fe/H] = +0.15; the distance moduli and any small age difference between these two clusters are irrelevant for purposes of the discussion. The combined Hyades/Praesepe samples are used to delineate an Li-dip profile, centered at $B-V = 0.44$ or 1.42 $M_{\odot}$. Evolution of the profile to the mean age of the three older clusters generates a CMD morphology that reproduces the observed Li-dip turnoff extremely well, implying that while the mass of stars in the center of the dip varies positively with metallicity, the color profile of Li-depletion across the dip may be similar but with the central color shifted to bluer values for lower [Fe/H]. Over the range from [Fe/H] $= -0.1$ to +0.15, the central mass of the dip follows the relation $M/M_{\odot} = 1.38\,(\pm0.04) + 0.4\,(\pm0.2)$[Fe/H]. Within the errors, there appears to be little change in the degree of Li-depletion for stars within the dip for ages greater than the Hyades. For lower mass stars just below the Li-dip, there is some evidence for modest depletion in Li ($\sim$0.2 dex) between 0.7 Gyr and 1.5 Gyr, assuming the clusters all formed with the same level of Li on the ZAMS. For the giants, the color and Li dichotomy discussed in previous investigations have been confirmed and strengthened for NGC 752 and NGC 3680. The younger cluster has, relative to the first-ascent giant branch, a significantly bluer giant branch distribution than NGC 3680, while only 2 of 11 stars have detectable Li falling within the $A(\mathrm{Li}) = 1$ bin, in contrast with 5 of 9 for NGC 3680. For IC 4651, the comparable numbers are 2 of 10, as expected given its similarity to NGC 752, but these claims are tempered by the uncertainty in the true Li abundance for three additional giants. If this pattern holds up, it strengthens the argument that, due to the lower mass of the stars leaving the main sequence, the giants populating the supposed clump in NGC 3680 are first-ascent giants, placing an important constraint on the transition in evolved structure for stars in the mass range of 1.8–1.6 $M_{\odot}$.

The three clusters profiled in this investigation are regularly compared because they are so similar but also because they represent objects that, by the standards of open cluster work, are well studied. The spectroscopic sample of stars within NGC 3680 has been doubled by this analysis but the Li-dip profile, as presented in Figure 10, can only be adequately mapped through the superposition of data from all three clusters. One reason for the frequently qualified conclusions in the present paper, as well as others related to Li evolution, is the small number of single members, as is the case in NGC 3680; in other clusters, the paucity of data represents an inadequate fraction of cluster members incorporated in analyses. As an example, the plateau effect for stars above the Li-dip seems apparent in Figure 10, but delineation of the brighter stars' depletion as they evolve toward the giant branch is hampered by observations of only one star in this region in NGC 752 and only five of more than two dozen possible candidates in IC 4651. A more complete set of observations has been obtained in NGC 752 by one of the authors (C.D.), but an expanded sample in IC 4651, especially among the giants, could prove invaluable.

In the arena of future observations, two needs come to mind. One of the weaknesses of the metallicity-dependent relation derived for the mass of the center of the Li-dip is the small baseline in [Fe/H]. A critical test of its reliability could come from the observation of a more metal-poor open cluster in a comparable age range. The obvious options are NGC 2420 and NGC 2506 with typical estimated abundances (Twarog

et al. 1997; Friel et al. 2002; Anthony-Twarog et al. 2006; Lee et al. 2008) between [Fe/H] = −0.3 and −0.4, though, for a higher estimate for NGC 2506, see Carretta et al. (2004). The second somewhat surprising deficiency is the lack of modern, broad-band, wide-field CCD photometry for two of the three clusters discussed: IC 4651 and NGC 752. The *uvby* survey of IC 4651 by Meibom (2000) is outstanding, but a complementary broad-band database would make isochrone comparisons more straightforward, particularly on the lower main sequence; the composite sample for NGC 752 clearly has a high but uneven degree of precision and remains incomplete at fainter magnitudes.

The authors thank the referee for thoughtful and constructive comments, and the staff at Cerro Tololo Inter-American Observatory for their invaluable assistance in obtaining the observations that form the basis of this study. CTIO is operated by the Association of Universities for Research in Astronomy, under contract with the National Science Foundation. Extensive use was made of the SIMBAD database, operating at CDS, Strasbourg, France and the WEBDA database maintained at the University of Vienna, Austria (http://www.univie.ac.at/webda). We also acknowledge with gratitude the use of IRAF, distributed by the National Optical Astronomy Observatories. C.P.D. gratefully acknowledges support from the National Science Foundation under grant AST-0607667. B.J.A.T. and B.A.T. are also grateful to the Astronomy Department at Indiana University for hospitality during their Fall 2008 stay in Bloomington.

REFERENCES

Alonso, R., Arribas, R., & Martinez-Roger, C. 1996, A&AS, 117, 227
Alonso, R., Arribas, R., & Martinez-Roger, C. 1999, A&AS, 140, 261
An, D., Terndrup, D. M., Pinsonneault, M. H., Paulson, D. B., Hanson, R. B., & Stauffer, J. R. 2007, ApJ, 655, 233
Anders, E., & Grevesse, N. 1989, Geochim. Cosmochim. Acta, 53, 197
Andersen, J., Clausen, J. V., & Nordström, B. 1990, ApJ, 363, L33
Anthony-Twarog, B. J., Heim, E. A., Twarog, B. J., & Caldwell, N. 1991, AJ, 102, 1056
Anthony-Twarog, B. J., Mukherjee, K., Caldwell, N., & Twarog, B. A. 1988, AJ, 95, 1453
Anthony-Twarog, B. J., Tanner, D., Cracraft, M., & Twarog, B. A. 2006, AJ, 131, 461
Anthony-Twarog, B. J., & Twarog, B. A. 1987, AJ, 94, 1222
Anthony-Twarog, B. J., & Twarog, B. A. 2000, AJ, 119, 2282
Anthony-Twarog, B. J., & Twarog, B. A. 2004, AJ, 127, 1000 (ATT)
Anthony-Twarog, B. J., & Twarog, B. A. 2006, PASP, 118, 358
Anthony-Twarog, B. J., Twarog, B. A., & Shodhan, S. 1989, AJ, 98, 1634
Ashwell, J. F., Jeffries, R. D., Smalley, B., Deliyannis, C. P., Steinhauer, A., & King, J. R. 2005, MNRAS, 363, L81
Bahcall, J. N., Pinsonneault, M. H., & Wasserburg, G. J. 1995, Rev. Mod. Phys., 67, 781
Balachandran, S. 1995, ApJ, 446, 203
Balachandran, S., Anthony-Twarog, B. J., & Twarog, B. A. 1991, in ASP Conf. Ser. 13, The Formation and Evolution of Star Clusters, ed. K. Janes (San Francisco, CA: ASP), 544
Biazzo, K., et al. 2007, A&A, 475, 981
Boesgaard, A. M. 1989, ApJ, 336, 798
Boesgaard, A. M., Armengaud, E., King, J. R., Deliyannis, C. P., & Stephens, A. 2004, ApJ, 613, 1202
Boesgaard, A. M., & Budge, K. G. 1988, ApJ, 332, 410
Boesgaard, A. M., Budge, K. G., & Ramsay, M. E. 1988, ApJ, 327, 389
Boesgaard, A. M., Deliyannis, C. P., King, J. R., & Stephens, A. 2001, ApJ, 533, 754
Boesgaard, A. M., Deliyannis, C. P., & Steinhauer, A. 2005, ApJ, 621, 991
Boesgaard, A. M., & King, J. R. 2002, ApJ, 565, 587
Boesgaard, A. M., & Tripicco, M. 1986a, ApJ, 302, L49
Boesgaard, A. M., & Tripicco, M. 1986b, ApJ, 303, 724
Bruntt, H., Frandsen, S., Kjeldsen, H., & Andersen, M. I. 1999, A&AS, 140, 135
Burkhart, C., & Coupry, M. F. 1998, A&A, 338, 1073
Carretta, E., Bragaglia, A., Gratton, R. G., & Tosi, M. 2004, A&A, 422, 991
Chaboyer, B., Demarque, P., Guenther, D. B., & Pinsonneault, M. H. 1995, ApJ, 446, 435
Charbonneau, P., & Michaud, G. 1988, ApJ, 334, 746
Charbonneau, P., & Michaud, G. 1990, ApJ, 352, 681
Charbonneau, P., Michaud, G., & Proffitt, C. R. 1989, ApJ, 347, 821
Charbonnel, C., & Talon, S. 2005, in EAS Publ. Ser. 17, Element Stratification in Stars: 40 Years of Atomic Diffusion, ed. G. Alecian, O. Richard, & S. Vauclair (Les Ulis: EDP), 167
Charbonnel, C., Vauclair, S., Maeder, A., Maynet, G., & Shaller, G. 1994, A&A, 283, 155
Chen, Y. Q., Nissen, P. E., Benoni, T., & Zhao, G. 2001, A&A, 371, 943
Clariá, J. J., & Lapasset, E. 1983, JA&A, 4, 117
Crawford, D. L., & Barnes, J. V. 1969, AJ, 74, 818
Crawford, D. L., & Barnes, J. V. 1970, AJ, 75, 946
Daniel, S. A., Latham, D. W., Mathieu, R. D., & Twarog, B. A. 1994, PASP, 106, 281
Deliyannis, C. P. 2000, in ASP Conf. Ser. 198, Stellar Clusters and Associations: Convection, Rotation and Dynamos, ed. R. Pallavicini, G. Micela, & S. Sciortino (San Francisco, CA: ASP), 235
Deliyannis, C. P., Boesgaard, A. M., Stephens, A., King, J. R., Vogt, S. S., & Keane, M. J. 1998, ApJ, 498, L147
Deliyannis, C. P., Demarque, P., & Kawaler, S. D. 1990, ApJS, 73, 21
Deliyannis, C. P., King, J. R., Boesgaard, A. M., & Ryan, S. G. 1994, ApJ, 434, L71
Deliyannis, C. P., & Pinsonneault, M. H. 1997, ApJ, 488, 836
Deliyannis, C. P., Pinsonneault, M. H., & Duncan, D. K. 1993, ApJ, 414, 740
Deliyannis, C. P., Steinhauer, A., & Jeffries, R. D. 2002, ApJ, 577, L39
Demarque, P., Woo, J.-H., Kim, Y.-C., & Yi, S. K. 2004, ApJS, 155, 667
do Nascimento, J. D., Jr., Canto Martins, B. L., Melo, C. H. F., Porto de Mello, G., & de Medeiros, J. R. 2003, A&A, 405, 723
Edvardsson, B., Anderson, J., Gustafsson, B., Lambert, D. L., Nissen, P. E., & Tomkin, J. 1993, A&A, 275, 101
Eggen, O. J. 1969, ApJ, 155, 439
Friel, E. D., & Boesgaard, A. M. 1992, ApJ, 387, 170
Friel, E. D., & Janes, K. A. 1993, A&A, 267, 75
Friel, E. D., Janes, K. A., Tavarez, M., Scott, J., Katsanis, R., Lotz, J., Hong, L., & Miller, N. 2002, AJ, 124, 2693
Garcia Lopez, R. J., & Spruit, H. C. 1991, ApJ, 377, 268
Geisler, D., Clará, J. J., & Minniti, D. 1991, AJ, 102, 1836
Girardi, L., Bertelli, G., Bressan, A., Chiosi, C., Groenewegen, M. A. T., Marigo, P., Salasnich, B., & Weiss, A. 2002, A&A, 391, 195
Hawley, S. L., Tourtellot, J. G., & Reid, I. N. 1999, AJ, 117, 1341
Hobbs, L. M., & Pilachowski, C. 1986, ApJ, 309, L17
Hobbs, L. M., & Thorburn, J. A. 1991, AJ, 102, 1070
Hobbs, L. M., & Thorburn, J. A. 1992, AJ, 104, 669
Houdek, G., & Gough, D. O. 2008, in IAU Symp. 252, The Art of Modelling Stars in the 21st Century, ed. L. Deng, K. L. Chan, & C. Chiosi (Dordrecht: Kluwer), 149
Jasniewicz, G., Recio-Blanco, A., de Laverny, P., Parthasarathy, M., & de Medeiros, J. R. 2006, A&A, 453, 717
Johnson, H. L. 1952, ApJ, 116, 640
Johnson, H. L., & Knuckles, C. F. 1955, ApJ, 122, 209
Joner, M. D., & Taylor, B. J. 1995, PASP, 107, 351
Joner, M. D., & Taylor, B. J. 2007, PASP, 119, 1093
Joner, M. D., Taylor, B. J., Laney, C. D., & Van Wyk, F. 2006, AJ, 132, 111
Jones, B. F., Fischer, D., & Soderblom, D. R. 1999, AJ, 117, 330
King, J. R., Krishnamurthi, A., & Pinsonneault, M. H. 2000, AJ, 119, 859
Kjeldsen, H., & Frandsen, S. 1991, A&AS, 87, 119
Korn, A. J., Grundahl, F., Richard, O., Barklem, P. S., Mashonkina, L., Collet, R., Piskunov, N., & Gustafsson, B. 2006, Nature, 442, 657
Kozhurina-Platais, V., Demarque, P., Platais, I., Orosz, J. A., & Barnes, S. 1997, AJ, 113, 1045
Kozhurina-Platais, V., Girard, M., Platais, I., & Van Altena, W. F. 1995, AJ, 109, 672
Laws, C., & Gonzalez, G. 2003, ApJ, 595, 1148
Lee, Y. S., et al. 2008, AJ, 136, 2050
Mallik, S. V., Parthasarathy, M., & Pati, A. K. 2003, A&A, 409, 251
Marigo, P., Girardi, L., Bressan, A., Groenewegen, M. A. T., Silva, L., & Granato, G. L. 2008, A&A, 482, 883
Mazzei, P., & Pigatto, L. 1988, A&A, 193, 148
Meibom, S. 2000, A&A, 361, 929
Meibom, S., Andersen, J., & Nordström, B. 2002, A&A, 386, 187
Mendoza, E. E. 1967, Bol. Obs. Tonanzintla Tacubaya, 4, 149
Mermilliod, J.-C., Andersen, J., Nordström, B., & Mayor, M. 1995, A&A, 299, 53

Michaud, G. 1986, ApJ, 302, 650
Nissen, P. E. 1988, A&A, 199, 146
Nissen, P. E., Twarog, B. A., & Crawford, D. L. 1987, AJ, 93, 634
Nordström, B., Andersen, J., & Andersen, M. I. 1996, A&AS, 118, 407
Nordström, B., Andersen, J., & Andersen, M. I. 1997, A&A, 322, 460
Pace, G., Pasquini, L., & Francois, P. 2008, A&A, 489, 403
Pasquini, L., Randich, S., & Pallavicini, R. 2001, A&A, 374, 1017 (PRP)
Pasquini, L., Randich, S., Zoccali, M., Hill, V., Charbonnel, C., & Nordström, B. 2004, A&A, 424, 951
Piatti, A. E., Clariá, J. J., & Bica, E. 1998, ApJS, 116, 263
Pilachowski, C., & Hobbs, L. M. 1988, PASP, 100, 336
Pinsonneault, M. H. 1997, ARA&A, 35, 557
Pinsonneault, M. H., Kawaler, S. D., & Demarque, P. 1990, ApJS, 74, 501
Prisinzano, L., & Randich, S. 2007, A&A, 475, 539
Proffitt, C. R., & Michaud, G. 1989, ApJ, 346, 976
Ramírez, I., & Meléndez, J. 2005, ApJ, 626, 465
Randich, S., Gratton, R., Pallavicini, R., Pasquini, L., & Carretta, E. 1999, A&A, 348, 487
Randich, S., Pasquini, L., & Pallavicini, R. 2000, A&A, 356, L25
Randich, S., Sestito, P., Primas, F., Pallavicini, R., & Pasquini, L. 2006, A&A, 450, 557
Richer, J., & Michaud, G. 1993, ApJ, 416, 312
Ryan, S. G., & Deliyannis, C. P. 1995, ApJ, 453, 819
Santos, N. C., Lovis, C., Pace, G., Melendez, J., & Naef, D. 2009, A&A, 493, 309
Schramm, D. N., Steigman, G., & Dearborn, D. S. P. 1990, ApJ, 259, L55
Sestito, P., Bragaglia, A., Randich, S., Pallavicini, R., Andrievsky, S. M., & Korotin, S. A. 2008, A&A, 488, 933
Sestito, P., & Randich, S. 2005, A&A, 442, 615
Sestito, P., Randich, S., & Pallavicini, R. 2004, A&A, 426, 809
Sills, A., & Deliyannis, C. P. 2000, ApJ, 544, 944
Smiljanic, R., Gauderon, R., North, P., Barbuy, B., Charbonnel, C., & Mowlavi, N. 2009, A&A, 502, 267
Soderblom, D. R., Oey, M. S., Johnson, D. R. H., & Stone, R. P. S. 1990, AJ, 99, 595
Soderblom, D. R., Stauffer, J. R., Hudon, J. D., & Jones, B. F. 1993, ApJS, 85, 315
Steinhauer, A. 2003, PhD thesis, Indiana Univ.
Steinhauer, A., & Deliyannis, C. P. 2004, ApJ, 614, L65
Swenson, F. J., Faulkner, J., Rogers, F. J., & Iglesias, C. A. 1994, ApJ, 425, 286
Talon, S., & Charbonnel, C. 2003, A&A, 405, 1025
Taylor, B. J. 2006, AJ, 132, 2453
Thorburn, J. A., Hobbs, L. M., Deliyannis, C. P., & Pinsonneault, M. H. 1993, ApJ, 415, 150
Twarog, B. A. 1983, ApJ, 267, 207
Twarog, B. A., Ashman, K. M., & Anthony-Twarog, B. J. 1997, AJ, 114, 2556
VandenBerg, D., & Stetson, P. B. 2004, PASP, 116, 997
Wilson, R. E. 1953, General Catalog of Radial Velocities, Carnegie Inst. Washington D.C. Publ. 601
Yi, S., Kim, Y.-C., & Demarque, P. 2003, ApJS, 144, 259
Yong, D., Carney, B. W., & Teixera de Almeida, M. L. 2005, AJ, 130, 597
Zahn, J.-P., & Bouchet, L. 1989, A&A, 223, 112